

The interplay of the metallosensor CueR with two distinct CopZ chaperones defines copper homeostasis in *Pseudomonas aeruginosa*

Lorena Novoa-Aponte¹, David Ramírez¹, and José M. Argüello^{1*}

From the ¹Department of Chemistry and Biochemistry, Worcester Polytechnic Institute, 60 Prescott St, Worcester, Massachusetts, 01609, United States of America

Running title: Cytoplasmic Cu⁺ distribution in *P. aeruginosa*

*To whom correspondence should be addressed: Dr. José M. Argüello, Department of Chemistry and Biochemistry, Worcester Polytechnic Institute, 60 Prescott St, Worcester, Massachusetts, 01605, United States of America. Phone: (508) 330-5169, e-mail: arguello@wpi.edu

Keywords: Copper, *Pseudomonas aeruginosa*, homeostasis, metal, metalloprotein, metal sensor, metallochaperone, transcriptional regulation, stress response.

ABSTRACT

Copper homeostasis in pathogenic bacteria is critical for cuproprotein assembly and virulence. However, *in vivo* biochemical analyses of these processes are challenging, which has prevented defining and quantifying the homeostatic interplay between Cu⁺-sensing transcriptional regulators, chaperones, and sequestering molecules. The cytoplasm of *Pseudomonas aeruginosa* contains a Cu⁺-sensing transcriptional regulator, CueR, and two homologous metal chaperones, CopZ1 and CopZ2, forming a unique system for studying Cu⁺ homeostasis. We found here that both chaperones exchange Cu⁺, albeit at a slow rate, reaching equilibrium after 3 h, a time much longer than *P. aeruginosa* duplication time. Therefore, they appeared as two separate cellular Cu⁺ pools. Although both chaperones transferred Cu⁺ to CueR *in vitro*, experiments *in vivo* indicated that CopZ1 metallates CueR, eliciting the translation of Cu⁺ efflux transporters involved in metal tolerance. Although this observation was consistent with the relative Cu⁺ affinities of the three proteins (CopZ1 < CueR < CopZ2), *in vitro* and *in silico* analyses also indicated a stronger interaction between CopZ1 and CueR that was independent of Cu⁺. In contrast, CopZ2 function was defined by its distinctly high abundance during Cu²⁺ stress. Under resting conditions, CopZ2 remained largely in its *apo* form. Metal stress quickly induced CopZ2 expression, and its *holo* form predominated, reaching levels commensurate with the cytoplasmic Cu⁺ levels. In

summary, these results show that CopZ1 acts as chaperone delivering Cu⁺ to the CueR sensor, whereas CopZ2 functions as a fast-response Cu⁺-sequestering storage protein. We propose that equivalent proteins likely play similar roles in most bacterial systems.

Copper is a micronutrient required as a redox co-factor by multiple enzymes (e.g., Cu-superoxide dismutases, cytochrome oxidases, etc.) (1-4). Nevertheless, free Cu⁺²⁺ is toxic as it disrupts Fe-S centers and generates free radicals (5,6). Copper antibacterial properties and role in innate immunity are the direct consequence of this cellular toxicity (7,8). These deleterious cellular effects have enabled the identification of molecules conferring tolerance to Cu⁺²⁺ in bacterial systems (1,9,10). These include cytoplasmic metal sensing transcriptional regulators, chaperone proteins, and transmembrane efflux systems. *In vitro* biochemical studies have shown high affinity Cu⁺ bind to these proteins leading to the virtual absence of unbound metal with Cu⁺ movement via ligand exchange among interacting proteins (1,9,11,12). These observations have not however produced an integrated description of the molecular interplay leading to cellular Cu⁺²⁺ homeostasis. This is, there is a conceptual gap between the phenotypical observations (effect of Cu⁺²⁺ on cell growth rate) and the biochemical characterization of isolated molecules. Consider for instance, the limited information on how Cu⁺ reaches compartmentally restricted target cupro-proteins or that no plasma

membrane transporters enabling Cu⁺²⁺ influx have been characterized, except for CcoA that provides copper for cytochrome *c* oxidase assembly (13). Further complicating the analysis, Cu⁺ distribution/sensing molecules are not ubiquitous, as different bacterial species have solved Cu⁺²⁺ tolerance using alternative strategies (1,7,9,14).

Assuming that copper homeostasis is enabled by an integrated molecular system distributing Cu⁺ to various targets, we characterized this molecular network in *Pseudomonas aeruginosa* under non-deleterious extracellular Cu²⁺ stress. This is, the system was studied under steady state conditions where Cu⁺ influx is equal to efflux, cells have the capacity to sequester cytoplasmic Cu⁺ excess, and there is not change on cellular growth rate (15). Genome-wide transcriptomic analysis revealed the presence of a cytoplasmic (CueR) and a periplasmic (CopS/R) Cu⁺ sensing regulators, their corresponding regulons, multiple metal chaperones, and specific Cu⁺ efflux and influx systems bridging the membranes separating cellular compartments (15). This was later complemented by mathematical simulation of fluxes and compartmental pools describing the experimental metal uptake kinetics (16). These computational models support novel homeostatic elements revealed by the architecture of the CueR and CopS/R regulons; for instance, the participation of the CusCBA system mobilizing cytoplasmic Cu⁺, or the significant role that periplasmic proteins might play in the response to external Cu²⁺. However, while these approaches gave an initial picture of the homeostatic network, they provided little information on the intra-compartmental metal distribution. How is Cu⁺ exchanged among soluble proteins in each compartment? Which molecules chaperone Cu⁺ and interact with the alternative transporters? How is the measured excess of Cu⁺ stored under steady state conditions?

Considering the fate of Cu⁺ in *P. aeruginosa* cytoplasm, the interplay of CueR and the two identified cytoplasmic metal chaperones appears key for the metal distribution. CueR is a member of the MerR family (17,18). It forms homodimers with three domains: A N-terminal DNA binding domain, a central dimerization helix, and a C-terminal region where two cysteines are responsible for metal binding (12,17). CueR

homologs bind Cu⁺ with 10⁻¹⁹-10⁻²¹ M affinities (12,19) and both forms of the regulator, CueR_{apo} and CueR_{holo}, bind the cognate promoter regions (20,21). The high binding affinity of the sensor has led to assume that there is no “free” cytoplasmic Cu⁺ (12). Quite relevant, it is unknown how CueR acquires the metal. Although CopZ-like Cu⁺ chaperones appear to deliver the metal to other transcriptional regulators such as CopY (22-24) and CsoR (25). Interestingly, *P. aeruginosa* genome encodes for two cytoplasmic Cu⁺ chaperones, CopZ1 and CopZ2 (15). Both are under control of CueR, binding Cu⁺ with 1:1 stoichiometry and high affinity, CopZ1 4 x 10⁻¹⁵ M and CopZ2 8 x 10⁻¹⁷ M (15). This multiplicity of copper chaperones has been also observed in *Streptomyces lividans* that has four CopZ-like Cu⁺ chaperones (25). Even though their Cu⁺ affinities have been determined (CopZ-1317 10⁻¹⁷ M and CopZ-3079 10⁻¹⁸ M), their possible function is obscure as they both appear to interact similarly with CsoR. A bioinformatic approach has also showed the presence of various CopZ homologous proteins in some *Rhizobiales* species and a correlation with multiple Cu⁺-ATPases encoded in the genomes was observed (26).

In this study, we report the distinct roles of *P. aeruginosa* Cu-chaperones, CopZ1 and CopZ2. *In vitro* and *in vivo* studies show that CopZ1 delivers metal to CueR via protein-protein interactions; while the more abundant CopZ2 serves as the Cu⁺ storage pool providing a fast-homeostatic response to high Cu⁺ level conditions. These properties provide a mechanistical model to explain the various equilibria among cytoplasmic Cu⁺ binding proteins and a novel strategy for Cu⁺ tolerance via metal binding to a cytoplasmic protein.

Results

CopZ1 and CopZ2 have distinct roles in *P. aeruginosa*. The structural similarities between CopZ1 and CopZ2, sharing 37% of sequence identity and the invariant CXXC Cu-binding motif, might suggest an analogous functional role. Analysis of 896 homologous sequences shows that these can be divided in two subgroups of chaperones. The CopZ1-like subgroup (544 sequences), including all eukaryotic chaperones, shows a conserved CXGC sequence in the metal binding region (Fig. 1A). Instead, CopZ2-like

proteins (352 sequences) are only present in prokaryotes and the Cu⁺ binding loop has an invariant His (MXCXHC) (Fig. 1B). This His is likely responsible for the higher Cu⁺ affinity observed in *P. aeruginosa* CopZ2 (15), as it has been shown that its removal decreases *S. lividans* CopZs affinity for Cu⁺ (25). Moreover, the His is probably determinant of their different behavior in the presence of Cu⁺ where CopZ2 (but not CopZ1) forms Cu⁺ mediated multimeric structures even with equimolar Cu⁺ as observed in native PAGE gels (Fig. 1C). It is known that in various conditions, chaperones form protein clusters binding multiple Cu⁺ ions (27-31). However, it is not our goal here to analyze these structures, but rather point out the different structural and Cu⁺ binding properties that might lead to the alternative roles shown below.

Searching for biological evidences of their distinct functions, we examined the contributions of *P. aeruginosa* CopZ1 and CopZ2 to the overall cellular tolerance to Cu⁺ stress. Strains carrying deletion mutants in the coding genes ($\Delta copZ1$, $\Delta copZ2$, and $\Delta copZ1/\Delta copZ2$) were grown in LB media containing various Cu²⁺ concentrations (Fig. 2A). The *P. aeruginosa* $\Delta copA1$ mutant strain lacking the Cu⁺-ATPase responsible for cytoplasmic Cu⁺ efflux was included as a control (32). In the absence of added metal, the growth rate of all strains was similar to that of the wild type (WT) cells. No significant differences were detected in the growth rate of $\Delta copZ1$ and $\Delta copZ2$ in the presence of low 0 - 3 mM Cu²⁺. However, the $\Delta copZ1$ mutant was more susceptible to metal toxicity at higher, 3.5 mM Cu²⁺ levels. A slightly more pronounced phenotype was observed in the double mutant $\Delta copZ1/\Delta copZ2$, while the susceptibility to Cu²⁺ was abrogated in the $\Delta copZ1::copZ1$ complemented strain. This altered tolerance to Cu²⁺ in $\Delta copZ1$ was similar to that observed for deletion mutants of homologous genes in *Bacillus subtilis*, *Agrobacterium tumefaciens*, and *Enterococcus hirae* (22,33-35); albeit, mutation of CopZ in *Listeria monocytogenes* and *P. fluorescens* did not lead to a diminished metal tolerance (36,37). The distinct growth phenotypes of $\Delta copZ1$ and $\Delta copZ2$ under Cu²⁺ stress were supported by determinations of whole cell Cu levels (Fig. 2B). Treatment of cells for 10 min with 0.5 mM CuSO₄ was chosen to

examine effects on the overall Cu homeostasis. We have shown that these conditions raise cellular Cu but do not affect cellular growth rates (15,16). Fig. 2B shows that all mutant stains presented small increments in basal Cu levels. More relevant, both $\Delta copZ1$ and $\Delta copZ1/\Delta copZ2$ mutant strains showed significantly higher levels of cellular Cu upon exposure to CuSO₄. On the other hand, the $\Delta copZ2$ mutation did not affect the cell copper levels paralleling its lack of growth phenotype. These differences in Cu²⁺ tolerance and cellular metal levels observed in $\Delta copZ1$ and $\Delta copZ2$ strains point out distinct functional roles for the corresponding proteins.

Cu⁺ exchange among CopZ1 and CopZ2. Cu⁺ transfer between homologous CopZ proteins and the structurally similar N-terminal metal binding domains present in Cu⁺-ATPases is well characterized (38-40). This hinted at a possible Cu⁺ exchange among CopZ1 and CopZ2; although, the large difference in their Cu⁺ affinities might limit metal transfer from CopZ2 to CopZ1 (CopZ2 $K_D = 8 \times 10^{-17}$ M; CopZ1 $K_D = 4 \times 10^{-15}$ M (15)). To explore the CopZs/Cu⁺ exchange, we performed bidirectional *in vitro* Cu⁺ transfer assays. This is, a CopZ was loaded with equimolar amounts of Cu⁺, incubated in the presence of its *apo* homolog, separated with affinity Ni-NTA resin, and Cu⁺ associated with each CopZ measured. All assays were performed in presence of reducing 10 mM ascorbic acid. Fig. 3A shows that CopZ1_{holo} transferred bound Cu⁺, although not all, to CopZ2_{apo}. Alternatively, as expected, a much-limited transfer was apparent from CopZ2_{holo} to CopZ1_{apo} (Fig. 3B). In both cases, control experiments performed in the absence of acceptor protein show that <5% of Cu⁺ was dissociated from *holo* donor after 10 min reaction (Fig. 3A-B). This is, the Cu⁺-exchange was not due to dissociation from donor and subsequent binding to acceptor. While these experiments show a predominant transfer of Cu⁺ from CopZ1 to CopZ2, it was apparent that equilibrium was not reached under the experimental conditions. The ratio of the CopZ1/CopZ2 Cu⁺ binding K_D yields a $K_{eq} = 42$; yet, if the levels of the CopZ1_{apo/holo} and CopZ2_{apo/holo} at the end of the 10 min exchange were considered, a reaction quotient smaller than that expected from the K_{eq} was observed (Fig. 3C).

Alternatively, longer Cu⁺ exchange experiments showed that after 3 h incubation, the reaction quotient for the exchange reaction reached a value of 53, quite close to the calculated K_{eq} . These data clearly show the anticipated Cu⁺ exchange and that the predicted equilibrium is eventually reached. This is, at equilibrium the CopZ2_{holo} predominates over CopZ1_{holo}. Perhaps more important, the data reveals a quite slow Cu⁺ exchange. Considering the *P. aeruginosa* duplication time of 25-35 min in LB media (41), it is apparent that the CopZ1/CopZ2 metal exchange would not reach equilibrium and that both chaperones would function as relatively independent Cu⁺ pools.

CueR receives Cu⁺ from both CopZ1 and CopZ2 *in vitro*. Cu⁺ transfer from CopZ-like chaperones to CueR has been assumed but not experimentally demonstrated; although chaperones supply the metal to other transcriptional regulators (22-25). This hypothesis was tested by measuring Cu⁺ transfer from the *holo* forms of CopZ1 and CopZ2 to CueR_{apo}. *P. aeruginosa* CueR was heterologously expressed and affinity purified. A limited fraction (10-12%) of the resulting protein contained bound Cu⁺ that could not be removed by extensive treatment with various chelators. The purified protein showed a high affinity for Cu⁺ ($K_D = 2.5 \pm 1.0 \times 10^{-16}$ M) (Fig. S1). Noticeably, this constant is lower than that reported for *E. coli* CueR (10⁻²¹ M) or *Salmonella enterica* CueR (3 x 10⁻¹⁹ M) and closer to that observed for other Cu⁺ sensors like *Streptococcus pneumoniae* CopY (10⁻¹⁷ M) or *Mycobacterium tuberculosis* (10⁻¹⁸ M) (12,19,42, 43). However, when compared in the context of CopZ1.Cu⁺ and CopZ2.Cu⁺ K_{DS} , the halfway CueR K_D hinted to possible different interactions with each chaperone.

Fig. 4A shows that both CopZ1_{holo} and CopZ2_{holo} deliver Cu⁺ to CueR_{apo}. However, CopZ1 appeared to transfer larger amounts of Cu⁺ to CueR, with a larger fraction of CopZ2 remaining in the *holo* form after the assay (CopZ1_{holo} 27±1%; CopZ2 63±1%; P<0.03). As in the CopZ1/CopZ2 exchange experiments (Fig. 3), no free Cu⁺ was detected in eluates from columns loaded with CopZ1_{holo} or CopZ2_{holo} in the absence of CueR (not shown). It has been shown that both CueR_{apo} and CueR_{holo} bind with similar dissociation constants the promoter region of genes under its control (44). Exploring the effect

of DNA binding on the CueR/CopZs interactions, the Cu⁺ transfer from CopZ1_{holo} or CopZ2_{holo} to CueR_{apo} bound to the promoter region of *copZ2* (*PcopZ2*) (Table S1) was also examined. The interaction CueR_{apo}-*PcopZ2* was confirmed using an electrophoretic mobility shift assay (Fig. S2). Again, both chaperones delivered Cu⁺ to the sensor and the transfer was not significantly different from the experiments in the absence of DNA (Fig. 4B). These results point out that the activation of CueR occurs via direct Cu⁺ transfer from the chaperones. Moreover, the data agree with the relative affinities of the three molecules for Cu⁺ (CopZ2 > CueR > CopZ1).

Stronger interaction of CueR with CopZ1. It has been shown that movement of Cu⁺ within a Cu⁺ homeostatic network occurs via highly specific protein-protein interactions ensuring the absence of free Cu⁺ (1,22-25,45). Exploring whether the metal transfer from chaperones to CueR is governed by structural aspects and metal affinities, we investigated the interaction of chaperones with CueR in the absence of metal. Co-purification of the proteins at increasing CueR:CopZs ratios showed a stronger interaction of CopZ1 with the sensor (Fig. 5), in agreement with the larger Cu⁺ transfer from CopZ1 to CueR (Fig. 4). This evidence was further supported by *in silico* docking experiments. These required modeling the *P. aeruginosa* molecules using structures of homologous proteins as templates. The available *E. coli* CueR_{apo} structure lacks the metal binding Cys in the C-terminal end of the protein and was not suitable for these studies (46). Consequently, CueR_{holo} was selected as docking receptor while *apo* forms of CopZs were used as ligands. *E. coli* CueR_{holo} was used to model *P. aeruginosa* CueR; while *S. typhimurium* GolB_{apo} and the *Thermus thermophilus* CopZ_{apo} served as templates of CopZ1 and CopZ2, respectively. It could be argued that the relevant dockings to consider were that of the *holo* forms of CopZs with the CueR_{apo}. However, the similarities of the *holo* and *apo* CopZs structures suggested that the calculated interactions would be quite similar for both forms (RMSD between GolB_{apo} (4Y2K) and GolB_{holo} (4Y2I) is 0.094 Å (47)). Furthermore, considering that only the protein:protein interactions would be analyzed, the metal ion was likely to play a minor role.

Docking simulations were restricted to a distance range of <10 Å between metal binding Cys in the chaperones and CueR. The best docking solutions were selected by applying a maximum 2 Å RMSD cut off, clustered, and ranked according to the HADDOCK score (Table S2) (48). This initial analysis clearly showed that the CueR_{holo}-CopZ1_{apo} pair conformers presented lower bonding (electrostatic and desolvation) energies when compared to the CueR_{holo}-CopZ2_{apo}. While these results indicated a more stable CueR-CopZ1 interaction, docking energies cannot be directly linked to binding free energies (48). Toward obtaining a more conclusive evaluation, the interacting residues at the protein interfaces (10 Å cut off) in each cluster were selected, their RMSDs calculated, and plotted against the HADDOCK score. Fig. 6A shows that in general CueR_{holo}-CopZ1_{apo} clusters of docking solutions had much lower i-l-RMSDs than the CueR_{holo}-CopZ2_{apo} clusters. This is, the proteins were closer, less disperse, in the CueR_{holo}-CopZ1_{apo} interactions. Moreover, if only those clusters statistically significant are considered (Clusters 1 and 10 Table S2, red dots Fig. 6A), the strength of the CueR_{holo}-CopZ1_{apo} interaction compared to CueR_{holo}-CopZ2_{apo} becomes more evident.

Fig. 6B shows a molecular model of the CueR_{holo}-CopZ1_{apo} interaction where a bonding network composed mainly by salt bridges and hydrogen bonds is observed. Again, comparison of these bonding interfaces shows the stronger interaction in the case of the CueR_{holo}-CopZ1_{apo} pair. Ten H-bonds and 7 salt bridges were observed at the CueR_{holo}-CopZ1_{apo} interface, while CueR_{holo}-CopZ2_{apo} presented 7H-bonds and 2 salt bridges (Table S3). In both cases, a common binding site in CueR (Glu110, Arg117, Asp119, Lys124, and Cys131) appeared to be involved in intermolecular hydrogen bonds and hydrophobic contacts.

In summary, *in vivo* and *in silico* analyses support the hypothesis that CopZ1 is the chaperone that interacts with and delivers the metal to CueR. Moreover, those indicate that the protein:protein recognition, independent of the Cu⁺ transfer event, has a contributing effect to the targeting and distribution of Cu⁺ within the cell.

CopZ1 mediates the transcriptional regulation of CopA1 expression. The described experiments suggest that CopZ1 might have a main role as Cu⁺ donor to CueR. Testing this idea, the dependence of CueR mediated transcription on CopZ1 and CopZ2 was studied *in vivo*. The expression of the *copA1* gene was used as reporter of CueR activity. CopA1 is the P-type ATPase responsible for cytoplasmic Cu⁺ efflux (32). The *P. aeruginosa copZ1*, *copZ2*, and *copA1* genes are all under control of CueR (15). As a first step in these experiments, their expression kinetic upon exposure to external 0.5 mM Cu²⁺ was determined. Fig. 7A shows that the transcriptional response to external Cu²⁺ takes place within 5 min of exposure. Importantly, an earlier increase in *copZ1* and *copZ2* transcript levels was observed followed by higher expression of *copA1*. Transcript levels decayed after 5 min exposure consistent with the system reaching steady state (15). It was also notable that expression levels of *copZ1* are substantially lower than those of *copZ2* (~ 8-times at 5 min). Based on these results, the expression of *copA1* in *P. aeruginosa* strains was measured after 2 min of exposure to Cu²⁺ (Fig. 7B). As previously shown, deletion of CueR completely abolished the expression of *copA1* (15). Most importantly, *copA1* expression was diminished in $\Delta copZ1$ while the $\Delta copZ2$ strain showed a slightly increased expression of the transporter. Cells lacking both *copZ1/copZ2* displayed an impaired phenotype similar to that of $\Delta copZ1$. Validating these results, complementation of the mutant strains resulted in restoration of the *copA1* expression. These results clearly support the role of CopZ1 delivering Cu⁺ to CueR to elicit the cellular response to increased Cu⁺ levels and argue against CopZ2 transferring Cu⁺ to CueR *in vivo*. Moreover, these observations explain the critical role of CopZ1, but not CopZ2, conferring tolerance to high (3.5 mM) external Cu²⁺ levels (Fig. 2). The higher expression of CopA1 in the $\Delta copZ2$ strain is in agreement with the role of CopZ2 shown in the following experiments.

CopZ2 is more abundant than CopZ1 *in vivo*. The described results show that CopZ1 supplies Cu⁺ for CueR activation. Then, what role does CopZ2 play in the response to Cu⁺ stress? The large transcriptional up-regulation of *copZ2* (Fig. 7A) indicates that CopZ2 abundance might rise

significantly in the presence of high intracellular Cu⁺. The *in vivo* levels of CopZ1 and CopZ2 were measured in mutant strains complemented with the corresponding gene carrying a 3' His-tag coding sequence under the control of its own promoter (500 bp upstream sequence). Distinct from other bacteria, *P. aeruginosa* *copZ* genes are located in single-gene operons, preceded by a CueR operator sequence (Fig. S3). Complemented strains were challenged with 0.5 mM Cu²⁺ and the produced His-tagged CopZs detected by immunostaining (Fig. 8). Resulting signals were calibrated with a standard curve of purified His-tagged protein. Fig. 8A shows that CopZ2 significantly more abundant than CopZ1 during the response to Cu⁺ stress. In fact, CopZ2 levels increased comparably to the intracellular Cu⁺ concentration (15). CopZ2 appeared as an early response to Cu⁺, reaching maximum protein levels 5-10 min after the initial exposure to Cu²⁺ (Fig. 8B). Importantly, chaperone levels remained elevated under steady state conditions again as the intracellular Cu⁺ content does (15). In contrast to CopZ2, CopZ1 showed a much more attenuated response to metal stress (Fig. 8A-B). CopZ1 increased 2-3 times while CopZ2 levels rise approximately 10 times (Fig. 8B). In bacteria, there is a strict cellular Cu quota, about 10⁴ atoms per cell (12), half or less are expected to be in the cytoplasm (16). These numbers correlate well with the amount of CopZ2 encountered in the cytoplasm during steady state, 40 fmol CopZ2 per μg of total protein. This represents a copy number of ~9,000 CopZ2 molecules per cell. While this is a rough estimation, is apparent that CopZ2 provides enough Cu⁺ storage in the cytoplasm, at least within certain ranges, during Cu⁺²⁺ stress.

CopZ2 is fully metallated upon Cu stress. The significant increase of CopZ2 upon Cu²⁺ exposure, suggests that this might act as a Cu⁺ buffer protein. Moreover, the small but sizable CopZ2 pool present at low Cu⁺ levels might serve as fast response preceding the synthesis of Cu⁺ efflux transporters. These ideas were examined by measuring the *apo/holo* ratio of each chaperone before and after 10 min stress with 0.5 mM Cu²⁺. In these experiments, again, mutant strains complemented with genes carrying His-tag coding sequences and under the control of their own promoters were used. After incubation in the

presence of Cu²⁺, cells were washed, homogenized in the presence of 10 mM maleimide and the levels of alkylated (*apo* form) and non non-alkylated (*holo* form) of the chaperones quantified by mass spectroscopy. Both chaperones contain Cys only in the Cu⁺ binding motifs (Fig. 1A-B), residues that are protected from maleimide alkylation when Cu⁺ is coordinated (Fig. S4). The relative increases of CopZ1 and CopZ2 levels upon Cu⁺ stress determined by mass spectrometry were comparable to those measured using immunostaining (Fig. S5).

Fig. 9 shows the *apo/holo* ratios of CopZ2 in cells growing in LB media with no added Cu²⁺ and for CopZ1 and CopZ2 upon Cu²⁺ exposure. Being a lower abundance chaperone, in the absence of external Cu²⁺, peptides containing the metal binding motif of CopZ1 were under the method detection limit and the relative levels of CopZ1_{holo} and CopZ1_{apo} could not be quantified. This was not the case in the presence of Cu²⁺, when CopZ1 was found fully metallated (Fig. 9A). Distinct was the case of CopZ2, that was observed partially metallated (44%) in the absence of Cu²⁺ but largely metallated (~98%) upon metal stress (Fig. 9B). Then, it is apparent that CopZ2 functions as a cytoplasmic Cu⁺ storage system of *P. aeruginosa*.

Exploring alternative cytoplasmic Cu⁺ sequestering mechanisms, other than CopZ2, we observed that no changes in glutathione levels are detected in the WT cells challenged with 0.5 mM Cu²⁺, nor in the Δ*copZ2* or Δ*copZ1/ΔcopZ2* mutant strains (Fig S6). Albeit, these mutants showed higher GSH basal levels. This agrees with our previous observations that Cu⁺ stress does not promote changes in the expression of glutathione biosynthesis genes, *PA2140* (metallothionein-like) or *csp3* gene (15). However, if CopZ2 plays a central role in the cytoplasmic Cu⁺ sequestration, how do bacteria overcome the absence of *copZ2* or why does the Δ*copZ2* strain show a normal Cu⁺ tolerance (Fig. 2A)? As shown in Fig. 7B, there is an elevated expression of *copA1* in the Δ*copZ2* strain. We hypothesize that this leads to a more efficient extrusion of Cu⁺ from the cytoplasm to compensate for a loss of chaperoning function. Then, the high affinity CopZ2 is likely to participate in the stabilization of Cu⁺ pools in the cytoplasm of *P. aeruginosa*.

Discussion

Bacterial Cu⁺²⁺ homeostasis is linked to a number of physiological processes through the metallation of key cuproenzymes including multicopper oxidases, cytochrome *c* oxidases, superoxide dismutase, nitrous oxide reductase, among others. Mechanisms of copper influx and efflux are, of course, instrumental to determine the cellular Cu⁺²⁺ quota. However, a basic analysis makes clear that Cu⁺²⁺ homeostasis is highly dependent on the metal cytoplasmic fate. In this compartment, the metal sensor is metallated and chaperones distribute metal to efflux transporters and cuproproteins. Moreover, various cytoplasmic molecules (GSH, Csp3, metallothionein) have been proposed to have a putative role in metal sequestration. Here, we report how the singular roles and interplay of two *P. aeruginosa* Cu⁺ chaperones, CopZ1 and CopZ2, enable the control of Cu⁺ homeostasis in the cytoplasmic compartment (Fig. 10). While metal exchange between the two chaperones is kinetically restricted (Fig. 3), CopZ1 metallates the sensor CueR (Fig. 4) and has a direct influence on the transcriptional control of the CueR regulon (Fig. 7), while CopZ2 sequester Cu⁺, acting in the fast response to Cu⁺ stress (Fig. 8-9).

Cu⁺ exchange among *P. aeruginosa* chaperones is kinetically restricted. Analysis of CopZ1 and CopZ2 structures, their distinct behavior binding metals and forming dimers (Fig. 1), and particularly the alternative phenotypes of mutant strains (Fig. 2), indicate that these proteins might have different cellular functions, and consequently constitute independent Cu⁺ pools. It has long been established that Cu⁺ chaperones exchange metal with structurally similar domains present in P_{1B1}-type ATPases (38-40). Then, Cu⁺ exchange among CopZ1 and CopZ2 could be expected such as they would reach a thermodynamic equilibrium dictated by their K_D for the metal. Results from CopZ1/CopZ2 Cu⁺ exchange experiments showed that while the metal exchange occurs, equilibrium is slowly reached after a few hours (Fig. 3). *P. aeruginosa* doubling time in rich media is 25-35 min. Then, it is probable that the CopZ1/CopZ2 Cu⁺ exchange operates far from equilibrium and the chaperones constitute two functionally separated metal pools.

CueR receives Cu⁺ from CopZ1. At the center of Cu⁺ homeostasis are the periplasmic and cytoplasmic metal sensors. CueR, a typical member of the MerR family, is the cytoplasmic Cu⁺ activated transcriptional regulator in *P. aeruginosa* (15,49). *Pa*CueR has a K_D one to three orders of magnitude larger than those reported for homologous proteins (12,19). However, CueR still satisfies the paradigm that there is no free Cu⁺ in the cell cytoplasm as one free Cu⁺ per cell would yield a 10⁻⁸ M concentration, formally eight orders of magnitude higher than the K_D of 2.5 x 10⁻¹⁶ M. Conversely, this K_D fits the observed interplay of CueR with CopZ1, that has a higher K_D (lower metal affinity), and CopZ2, which has a lower K_D .

Several lines of evidence show that CueR obtains Cu⁺ from CopZ1. We observed that *in vitro* CopZ1_{holo} transfers Cu⁺ to the CueR_{apo}. Moreover, CopZ1_{holo} is more efficient than CopZ2_{holo} metallating CueR_{apo} (Fig. 4). In principle, this observation could be just due to the relative K_D s of sensor and chaperones; this is the selectivity would be driven only by the relative Cu⁺ binding constants. In fact, metallation from a chaperone with lower affinity for Cu⁺ than the sensor appears to be the case in *S. pneumoniae* for CupA(site 2)/CopY (42,50). However, *in vitro* and *in silico* experiments showed that, largely independent of the metal ion, the transcription factor interacts more favorably with CopZ1 than CopZ2 (Fig. 5-6). Then, it is apparent that the protein:protein interaction should be thermodynamically shallow for CopZ1:CueR. These physicochemical principles driving the molecular behavior explain the *in vivo* control of *copA1* transcription by CopZ1 but not by CopZ2 (Fig. 7). This is particularly relevant under conditions of Cu⁺ stress when the pool of CopZ2 is roughly one order of magnitude higher than that of CopZ1 (Fig. 8).

CopZ2 serves as a Cu⁺ sequestering pool. The participation of Cu⁺ sequestering molecules in mechanisms of metal tolerance has been postulated (51). Among these, GSH, metallothionein (PA2140) and Cps3 (PA2107) are present in *P. aeruginosa*. However, none of these genes or enzymes related to GSH biosynthesis are induced during the exposure of *P. aeruginosa* to Cu²⁺, even though under these conditions cells reach four times higher Cu²⁺ levels compared to resting

conditions (15). Moreover, GSH levels do not increase during exposure to 0.5 mM Cu²⁺ (Fig. S6), nor the $\Delta csp3$ mutant strains is sensitive to high Cu²⁺ levels (not shown). Alternatively, upon *P. aeruginosa* exposure to 0.5 mM Cu²⁺ we observed a high induction of *copZ2* that resulted in large increase in CopZ2 proteins pools (Fig. 7-8). The manner the system integrates the cytoplasmic copper homeostatic network is interesting (Fig. 10). Under resting conditions both CopZ1 and CopZ2 appear to be at similar levels and CopZ2 is only partially metallated (Fig. 10, left panel). Upon Cu²⁺ stress, CopZ1 metallates the sensor CueR leading to transcriptional activation of the CueR regulon genes, including *copZ1*, *copZ2* and *copA1* (Fig. 10, central panel). The CopZ2 pool increases immediately and CopZ1 remains quite close to basal levels while both chaperones however are fully metallated (Fig. 10, right panel). Rough estimations suggest that the levels of CopZ2 might suffice to sequester all the Cu⁺ excess under the tested experimental conditions. In addition, the fast increase in CopZ2 together with the slow rate of metal exchange support the idea that both chaperones constitute independent Cu⁺ pools. While this idea is relevant when considering cytoplasmic Cu⁺ homeostasis, it is likely to have important implications for Cu⁺ distribution to cuproproteins and membrane transporters.

In summary, this study provides a novel model for copper homeostasis in bacteria. In *P. aeruginosa* the fate of cytoplasmic Cu⁺ is determined by the interplay between the metallosensor CueR and two CopZ chaperones (Fig. 10). CopZ1 acts as chaperone delivering Cu⁺ to the CueR sensor, while CopZ2 functions as fast response Cu⁺ sequestering system.

Experimental procedures

Bacterial strains. Bacterial strains, plasmids, and oligonucleotides used in this study are listed in Table S1. *P. aeruginosa* PAO1 served as WT strain. *P. aeruginosa* strains were grown at 37°C in LB medium supplemented 25 µg/mL irgasan (WT and mutant strains) or 30 µg/mL gentamicin (complemented strains). *Escherichia coli* strains were grown at 37°C in LB medium supplemented with 30 µg/mL kanamycin, 100 µg/mL ampicillin, or 10 µg/mL gentamicin, depending on the plasmids selection.

Construction of *P. aeruginosa* mutant and complemented strains. $\Delta copZ1$ mutant strain was a gift from Dr. S. Lory (Harvard Med. Sch.) (49). $\Delta copZ2$ and $\Delta copZ1/\Delta copZ2$ double mutant strains were constructed using the two-step allelic exchange method (52). Briefly, 500 bp regions flanking the *copZ2* gene were amplified by PCR. Mutant allele resulted from splicing by overlapping-PCR. A mutation replacing Cu-binding Cys for Ala residues, followed by a stop codon and a *PvuII* site were introduced to produce a non-functional *copZ2* mutant allele. This was cloned into the allelic exchange vector pDONRPEX18Gm, transformed into the donor *E. coli* S17.1, and transferred into the WT or $\Delta copZ1$ strains by conjugation. Single-crossover mutants were selected in 10 µg/mL gentamicin LB plates, and unmarked double-crossover mutants were isolated by counter-selection in 15% sucrose no salt-LB plates. Double-crossover bacterial strains were selected in 25 µg/mL irgasan, LB agar and screened by restriction digest of PCR products. Deletions were confirmed by sequencing.

Mutant strains were complemented with the corresponding gene carrying a 3'-His-tag coding sequence under control of the native promoter using the mini-Tn7 insertion system (53). The genes and their 500 bp upstream promoter regions were amplified by PCR. The 3' primer included a His-tag coding sequence. Amplicons were cloned into a pUC18-mini-Tn7-Gm vector. Resulting plasmids and helper plasmid pTNS2 were co-transformed into the corresponding $\Delta copZ1$ or $\Delta copZ2$ strain, followed by selection in 30 µg/mL gentamicin, LB plates. Complemented strains were verified by PCR.

Cu²⁺ sensitivity assay. Overnight cultures were diluted in 25 µg/mL irgasan, LB medium, adjusted to 0.05 OD₆₀₀, and supplemented with the indicated CuSO₄ concentration. Cell growth (OD₆₀₀) was monitored every 10 min for 10 h using an Epoch 2 Microplate Spectrophotometer (BioTek) at 37°C with continuous shaking. Cu uptake was measured in whole cells using atomic absorption spectroscopy (AAS) as described (15).

Protein expression and purification. CopZ1 and CopZ2 containing a His₆-tag joined by a TEV cleavage site were expressed in *E. coli* BL21(DE3)pLysS cells and purified as described

(15). When required, purified protein was subjected to TEV protease cleavage overnight and reapplied to the Ni-NTA column to obtain untagged proteins. Flow-through fractions were collected and buffer exchanged in 3 kDa centricons to 25 mM HEPES (pH 8), 100 mM sucrose, 150 mM NaCl and 1 mM DTT.

The *cueR* (PA4778) gene was amplified from genomic DNA using a 3'-end primer that introduced a Strep-tag coding sequence and a stop codon, cloned into a pBAD-topo vector (Invitrogen) and expressed in *E. coli* BL21(DE3) cells. CueR was affinity purified using Strep-Tactin[®]XT Superflow[®] columns (IBA). Isolated CueR contained 0.08-0.12 equivalents of Cu bound. Attempts to remove the residual Cu with combinations of metal chelators (TTM, KCN, BCS, EDTA) were not successful.

Purified proteins were stored in 20% glycerol, 25 mM HEPES (pH 8), 100 mM sucrose, 150 mM NaCl and 1 mM DTT at -80°C. Protein concentrations were determined in accordance to Bradford (54), thiol levels measured using Ellman's method (55), and bound Cu⁺ determined by AAS (15). In all cases, protein purity was ≥90% as estimated by SDS-PAGE followed by Coomassie brilliant blue staining. CopZs oligomerization was analyzed by Blue Native PAGE electrophoresis (56).

Cu⁺ binding and transfer. Cu⁺ loaded proteins were prepared by slow addition of CuSO₄ in the presence of 10 mM ascorbic acid to reduced proteins (3 h preincubation in 5 mM TCEP, 4°C). Unbound Cu⁺ was removed by passage through Sephadex PD-10 columns (CueR) or by washing after binding to Ni-NTA resin (CopZ1 and CopZ2). Cu⁺ transfer reactions were performed using *apo/holo* partners with different tags. 10 nmol of His-tagged CopZs_{holo} were incubated 30 min with Ni-NTA resin. Unbound protein and free Cu⁺ were washed with 20 mM imidazole, buffer H (25 mM HEPES (pH 8), 150 mM NaCl, 10 mM ascorbic acid). 10 nmol TEV-protease cleaved CopZs_{apo}, or 5 nmol of the Strep-tag CueR_{apo} dimer in the presence or absence of 5 nmol *PcopZ2* (dsDNA *copZ2* promoter region) were incubated 10 min at RT with resin bound CopZs_{holo}. Untagged proteins were collected in the washes with 20 mM imidazole, buffer H. His-

tagged proteins were eluted with 300 mM imidazole, buffer H. Eluted proteins were verified by SDS-PAGE/ Western blots immunostained with primary rabbit His-tag antibody, pAb, and goat anti-rabbit IgG antibody-horseradish peroxidase (GeneScript), or Strep-Tactin[®]-HRP conjugate (IBA). Eluted DNA was observed by agarose gel electrophoresis.

***In vitro* interaction of CueR with CopZ1 and CopZ2.** Interactions between regulator and chaperones were studied by assessing the co-purification of isolated proteins by batch affinity chromatography. 10 μM Strep-tagged CueR_{apo} dimer were incubated 10 min at room temperature with 10-100 μM His-tagged CopZs_{apo} in buffer containing 25 mM Tris-HCl (pH 8.0), 150 mM NaCl, 50 mM sucrose, 5 mM DTT, 0.2 mM BCS. Samples were incubated 10 min with 50 μL of Strep-Tactin[®]XT Superflow[®] resin (IBA) and centrifuged at 14000 rpm for 1 min to collect unbound proteins in the supernatant. Resins were washed twice with buffer 25 mM Tris-HCl (pH 8.0), 150 mM NaCl and bound proteins eluted with buffer supplemented with 50 mM Biotin. Controls were performed by individually subjecting each CopZ to the same protocol, lacking the interacting partner. Bound proteins were loaded onto nitrocellulose blotting-membrane and His-tagged proteins were immunostained as described above. Stained dots were recorded using ChemiDoc XRS+ Imager (BioRad), and quantified using the Gilles Carpentier-Dot Blot Analyzer for ImageJ (57).

Gene expression analysis. Cells (mid-exponential phase) were incubated in 0.5 mM CuSO₄ antibiotic-free LB medium. 0.5 mL aliquots were taken at indicated times, stabilized with RNA protect Bacteria Reagent (Qiagen), and RNA isolated with RNeasy Mini Kit (Qiagen). RNA was treated with DNase I, purified by phenol/chloroform extraction and ethanol precipitated. 1 μg of RNA was used for cDNA synthesis using the ProtoScript[®] II kit (New England BioLabs). qPCR reactions were carried out with FastStart Essential DNA Green Master (Roche) in 10 μL final volume, using 0.25 μM of each primer. The efficiency of primer sets was evaluated by qPCR in serial dilutions of WT cDNA. Results were normalized to 30S ribosomal

protein S12 (PA4268) (32). The Pfaffli method was used to compare samples (58).

CopZ1 and CopZ2 expression kinetics. CopZ1 and CopZ2 complemented strains (mid-exponential phase) were incubated in 0.5 mM CuSO₄ antibiotic-free LB medium and 2 mL aliquots were taken at indicated times. Cell pellets were resuspended in buffer 25 mM Tris-HCl (pH 7.4), 150 mM NaCl, 0.3% SDS, and sonicated twice on ice. Supernatants were adjusted to 4 µg/µL total protein, and 40 µg protein samples were loaded onto nitrocellulose blotting-membrane. As standard, a curve of 5-100 ng His-tagged pure protein was also included in the blot. His-tagged proteins were detected as described above. Stained dots were quantified as described above.

***In vivo* CopZ1 and CopZ2 apo-holo equilibrium determinations**

Protein alkylation and sample enrichment. CopZ1 and CopZ2 complemented strains (mid-exponential phase) were incubated in 0.5 mM CuSO₄ antibiotic-free LB medium, 10 min at 37°C. Cells were harvested by centrifugation (11,000 rpm, 3 min, 4°C), pellets resuspended in 25 mM Tris-HCl (pH 7.4), 150 mM NaCl, 10 mM maleimide and sonicated three times/30 sec in a dry-ice/ethanol bath. Alkylation reaction was stopped after 10 min incubation on ice by adding 20 mM L-cysteine. Cellular debris were removed by centrifugation at 16,000 rpm for 10 min at 4°C, and supernatants loaded into Ni-NTA columns. The collected His-tagged CopZs enriched fractions were concentrated in 3 kDa centricons.

In-solution digestion and LC-MS/MS analyses. Mass spectroscopy analysis was performed by the University of Massachusetts Mass Spectrometry Facility. CopZs enriched fractions were lyophilized, treated with in 0.1% Protease Max (Promega), reduced with 2.25 mM DTT, alkylated with 5 mM iodoacetamide, and digested with 0.4 µg trypsin (Promega). Peptides were cleaned using C18 zip-tips (OMIX), eluted in 80% acetonitrile, 1% formic acid, lyophilized, and re-suspended in 5% acetonitrile, 0.1% TFA. Peptides were analyzed by LC-MS/MS using a Waters NanoAcquity UPLC coupled to a Thermo Scientific Q Exactive Hybrid Quadrupole-Orbitrap mass spectrometer. Samples were loaded onto 100

µm ID fused-silica pre-column packed with Magic C18AQ 2 cm x 5 µm (200 Å) (Bruker-Michrom) at a flow rate of 4.0 µL/min for 4 min with 5% acetonitrile, 0.1% formic acid. Peptides were eluted at 300 nL/min from a 75 µm x 25 cm Magic C18AQ 3 µm (100 Å) particles with a linear gradient from 5-35% of mobile phase B (acetonitrile, 0.1% formic acid) in mobile phase A (0.1% formic acid), over 60 min. Ions were introduced by positive electrospray ionization into the Q Exactive. Full MS scans from 300-1750 *m/z* were acquired followed by 10 MS/MS scans acquired under HCD fragmentation at a resolution of 17,500 (*m/z* 200).

Data analysis. Raw data files were processed with Proteome Discoverer (Thermo), and identified using Mascot Server (version 2.4) against the *P. aeruginosa* SwissProt FASTA file (manually updated to include the CopZ2 protein). Search parameters included variable modifications of carbamidomethyl cysteine (Cam-Cys) and maleimide cysteine (Mal-Cys). Tolerance for assignments was restricted to 10 ppm for precursors and 0.05 Da for fragments. Results were processed by Scaffold (Proteome Software, Inc.) utilizing the Trans-Proteomic Pipeline (Institute for Systems Biology) with threshold values set at 95% for peptides (0.1% false-discovery rate) and 99% for proteins (2 peptides minimum). The *apo* and *holo* ratios of the proteins were quantified by summing the fragment intensity to obtain the molar fraction of modified (Mal) vs. non-modified (Cam) cysteines in Cu binding site-containing peptides.

Computational studies

Conserved residues in Cu-binding regions of CopZ-like chaperones. *P. aeruginosa* CopZs sequences were used as templates for BLAST searches of the non-redundant protein sequences database. *Pseudomonas* organisms were excluded. Sequences were sorted based on their Cu⁺ binding regions, CopZ1-like MxCxGC (543 sequences) or CopZ2-like MxCxHC (349 sequences). Both groups were aligned using the Muscle tool (Jalview) (59). Sequence logos were created using the WebLogo online tool (60).

Comparative modeling. Models of *P. aeruginosa* CueR_{holo}, CopZ1_{apo} and CopZ2_{apo} models were built using *E. coli* (Ag⁺)CueR (PDB ID: 4WLW)

(46); *Salmonella typhimurium* GolB (PDB ID: 4Y2K) (61) for CopZ1, and the *Thermus thermophilus* CopZ (PDB ID: 2ROE) (62) for CopZ2, as templates. Selected proteins share 48%, 45% and 42% of sequence identity with their *P. aeruginosa* homologues, respectively. Models were built using PRIME and optimized with Maestro protein preparation wizard (63). For protein-protein docking simulations, the Cu⁺ atom was kept in the metal binding site of the CueR protein. The PROPKA program was employed to set the protonation states at pH 7.0 and structures were energy minimized using PRIME (64).

Protein-protein docking simulations were done using the HADDOCK2.2 server (<https://haddock.science.uu.nl/services/HADDOCK2.2/>) (65). CueR_{holo} was selected as receptor and apo chaperones were chosen as ligands. Chaperone Cu⁺ binding Cys were placed within 10 Å of CueR Cu⁺ binding residues (Cys¹¹² and Cys¹²⁰) as

starting receptor-ligand positions (46). The CueR residues Glu¹¹⁰, His¹¹¹, Gln¹¹³, Arg¹¹⁷, Asp¹¹⁹, Pro¹²¹, and Lys¹²⁴ were set as active residues (allegedly directly involved in the interaction). For the chaperones CopZ1/CopZ2, residues Asn/Gly⁸, Thr¹⁰, Cys¹¹, Gly/His¹³, Cys¹⁴, Lys/Arg¹⁶, Arg³⁸, Ala/Glu⁵⁸, Gly⁵⁹, and Thr⁶⁰ were selected as active residues. Passive residues were automatically defined around the active residues. Docking simulations were performed using the default parameters of the server easy interface. The top-200 docking solutions were clustered based on the fraction of common contacts (FCC), with a cutoff of 0.75 and clusters ranked according to the HADDOCK score for further analysis. Protein: protein interactions in the best conformations (according to the HADDOCK score) of each cluster were analyzed using PISA (66). The interactions of the best CueR_{holo}-CopZ1 conformation were represented using PyMol (67).

Acknowledgments: This work was supported by a grant from the National Institutes of Health (R01GM114949 to J.M.A.). The authors thank the Center for Bioinformatics and Molecular Simulation – Universidad de Talca for the use of its computational resources. The authors thank Dr. Robert Dempski (Worcester Polytechnic Institute) and Dr. Daniel Raimunda (Instituto Investigación Médica Mercedes y Martín Ferreyra, CONICET-UNC) for critical reading of the manuscript and helpful discussions.

Conflicts of interest: The authors declare that they have no conflicts of interest with the contents of this article. The content is solely the responsibility of the authors and does not necessarily represent the official views of the National Institutes of Health.

References

1. Argüello, J. M., Raimunda, D., and Padilla-Benavides, T. (2013) Mechanisms of copper homeostasis in bacteria. *Front. Cell Infect. Microbiol.* **3**, 1-14
2. Fraústo da Silva, J. J. R., and Williams, R. J. P. (2001) *The Biological Chemistry of the Elements : the Inorganic Chemistry of Life*, 2nd ed., Oxford University Press, Oxford
3. Desideri, A., and Falconi, M. (2003) Prokaryotic Cu,Zn superoxidies dismutases. *Biochem. Soc. Trans.* **31**, 1322-1325
4. Brunori, M., Giuffrè, A., and Sarti, P. (2005) Cytochrome *c* oxidase, ligands and electrons. *J. Inorg. Biochem.* **99**, 324-336
5. Macomber, L., and Imlay, J. A. (2009) The iron-sulfur clusters of dehydratases are primary intracellular targets of copper toxicity. *Proc. Natl. Acad. Sci. USA* **106**, 8344-8349
6. Dupont, C. L., Grass, G., and Rensing, C. (2011) Copper toxicity and the origin of bacterial resistance-new insights and applications. *Metallomics* **3**, 1109-1118
7. Ladomersky, E., and Petris, M. J. (2015) Copper tolerance and virulence in bacteria. *Metallomics* **7**, 957-964
8. Hodgkinson, V., and Petris, M. J. (2012) Copper homeostasis at the host-pathogen interface. *J. Biol. Chem.* **287**, 13549-13555
9. Osman, D., and Cavet, J. S. (2008) Copper homeostasis in bacteria. *Adv. Appl. Microbiol.* **65**, 217-247
10. Rensing, C., and Grass, G. (2003) *Escherichia coli* mechanisms of copper homeostasis in a changing environment. *FEMS Microbiol. Rev.* **27**, 197-213
11. Argüello, J. M., Patel, S. J., and Quintana, J. (2016) Bacterial Cu⁺-ATPases: models for molecular structure-function studies. *Metallomics* **8**, 906-914
12. Changela, A., Chen, K., Xue, Y., Holschen, J., Outten, C. E., O'Halloran, T. V., and Mondragon, A. (2003) Molecular basis of metal-ion selectivity and zeptomolar sensitivity by CueR. *Science* **301**, 1383-1387
13. Ekici, S., Yang, H., Koch, H. G., and Daldal, F. (2012) Novel transporter required for biogenesis of *cbb3*-type cytochrome *c* oxidase in *Rhodobacter capsulatus*. *MBio.* **3**, e00293-00211
14. Hernández-Montes, G., Argüello, J. M., and Valderrama, B. (2012) Evolution and diversity of periplasmic proteins involved in copper homeostasis in gamma proteobacteria. *BMC Microbiol.* **12**, 249-263
15. Quintana, J., Novoa-Aponte, L., and Argüello, J. M. (2017) Copper homeostasis networks in the bacterium *Pseudomonas aeruginosa*. *J. Biol. Chem.* **292**, 15691-15704
16. Parmar, J. H., Quintana, J., Laubenbacher, R., Argüello, J. M., and Mendes, P. (2018) An important role for periplasmic storage in *Pseudomonas aeruginosa* copper homeostasis revealed by a combined experimental and computational modeling study. *Mol. Microbiol.* **110**, 357-369
17. Brown, N. L., Stoyanov, J. V., Kidd, S. P., and Hobman, J. L. (2003) The MerR family of transcriptional regulators. *FEMS Microbiol. Rev.* **27**, 145-163
18. Ma, Z., Jacobsen, F. E., and Giedroc, D. P. (2009) Coordination chemistry of bacterial metal transport and sensing. *Chem. Rev.* **109**, 4644-4681
19. Osman, D., Piergentili, C., Chen, J., Chakrabarti, B., Foster, A. W., Lurie-Luke, E., Huggins, T. G., and Robinson, N. J. (2015) Generating a metal-responsive transcriptional regulator to test what confers metal-sensing in cells. *J. Biol. Chem.*, jbc. M115. 663427
20. Chen, P., Keller, A. M., Joshi, C. P., Martell, D. J., Andoy, N. M., Benitez, J. J., Chen, T. Y., Santiago, A. G., and Yang, F. (2013) Single-molecule dynamics and mechanisms of metalloregulators and metallochaperones. *Biochemistry* **52**, 7170-7183
21. Outten, F. W., Outten, C. E., Hale, J., and O'Halloran, T. V. (2000) Transcriptional activation of an *Escherichia coli* copper efflux regulon by the chromosomal MerR homologue, CueR. *J. Biol. Chem.* **275**, 31024-31029

22. Odermatt, A., and Solioz, M. (1995) Two trans-acting metalloregulatory proteins controlling expression of the copper-ATPases of *Enterococcus hirae*. *J. Biol. Chem.* **270**, 4349-4354
23. Cobine, P., Wickramasinghe, W. A., Harrison, M. D., Weber, T., Solioz, M., and Dameron, C. T. (1999) The *Enterococcus hirae* copper chaperone CopZ delivers copper(I) to the CopY repressor. *FEBS Lett.* **445**, 27-30
24. Neubert, M. J., Dahlmann, E. A., Ambrose, A., and Johnson, M. D. (2017) Copper Chaperone CupA and Zinc Control CopY Regulation of the *Pneumococcal cop* Operon. *mSphere* **2**, e00372-00317
25. Chaplin, A. K., Tan, B. G., Vijgenboom, E., and Worrall, J. A. (2015) Copper trafficking in the CsoR regulon of *Streptomyces lividans*. *Metallomics* **7**, 145-155
26. Cubillas, C., Miranda-Sanchez, F., Gonzalez-Sanchez, A., Elizalde, J. P., Vinuesa, P., Brom, S., and Garcia-de Los Santos, A. (2017) A comprehensive phylogenetic analysis of copper transporting P_{1B} ATPases from bacteria of the *Rhizobiales* order uncovers multiplicity, diversity and novel taxonomic subtypes. *MicrobiologyOpen*
27. Kihlken, M. A., and Leech, A. P. (2002) Copper-mediated dimerization of CopZ, a predicted copper chaperone from *Bacillus subtilis*. *Biochem. J.* **368**, 729-739
28. Banci, L., Bertini, I., Del Conte, R., Mangani, S., and Meyer-Klaucke, W. (2003) X-ray absorption and NMR spectroscopic studies of CopZ, a copper chaperone in *Bacillus subtilis*: the coordination properties of the copper ion. *Biochemistry*. **42**, 2467-2474
29. Urvoas, A., Moutiez, M., Estienne, C., Couprie, J., Mintz, E., and Le Clainche, L. (2004) Metal-binding stoichiometry and selectivity of the copper chaperone CopZ from *Enterococcus hirae*. *Eur. J. Biochem.* **271**, 993-1003
30. Hearnshaw, S., West, C., Singleton, C., Zhou, L., Kihlken, M. A., Strange, R. W., Le Brun, N. E., and Hemmings, A. M. (2009) A tetranuclear Cu(I) cluster in the metallochaperone protein CopZ. *Biochemistry* **48**, 9324-9326
31. Kay, K. L., Hamilton, C. J., and Le Brun, N. E. (2016) Mass spectrometry of *B. subtilis* CopZ: Cu (I)-binding and interactions with bacillithiol. *Metallomics* **8**, 709-719
32. González-Guerrero, M., Raimunda, D., Cheng, X., and Argüello, J. M. (2010) Distinct functional roles of homologous Cu⁺ efflux ATPases in *Pseudomonas aeruginosa*. *Mol. Microbiol.* **78**, 1246-1258
33. Radford, D. S., Kihlken, M. A., Borrelly, G. P., Harwood, C. R., Le Brun, N. E., and Cavet, J. S. (2003) CopZ from *Bacillus subtilis* interacts *in vivo* with a copper exporting CPx-type ATPase CopA. *FEMS Microbiol. Lett.* **220**, 105-112
34. Gaballa, A., and Helmann, J. D. (2003) *Bacillus subtilis* CPx-type ATPases: Characterization of Cd, Zn, Co and Cu efflux systems. *Biometals* **16**, 497-505
35. Nawapan, S., Charoenlap, N., Charoenwuttitam, A., Saenkham, P., Mongkolsuk, S., and Vattanaviboon, P. (2009) Functional and expression analyses of the *cop* operon, required for copper resistance in *Agrobacterium tumefaciens*. *J. Bacteriol.* **191**, 5159-5168
36. Corbett, D., Schuler, S., Glenn, S., Andrew, P. W., Cavet, J. S., and Roberts, I. S. (2011) The combined actions of the copper-responsive repressor CsoR and copper-metallochaperone CopZ modulate CopA-mediated copper efflux in the intracellular pathogen *Listeria monocytogenes*. *Mol. Microbiol.* **81**, 457-472
37. Zhang, X. X., and Rainey, P. B. (2008) Regulation of copper homeostasis in *Pseudomonas fluorescens* SBW25. *Environ. Microbiol.* **10**, 3284-3294
38. Lutsenko, S. (2010) Human copper homeostasis: a network of interconnected pathways. *Curr. Opin. Chem. Biol.* **14**, 211-217
39. Banci, L., Bertini, I., McGreevy, K. S., and Rosato, A. (2010) Molecular recognition in copper trafficking. *Nat. Prod. Rep.* **27**, 695-710
40. Boal, A. K., and Rosenzweig, A. C. (2009) Structural biology of copper trafficking. *Chem. Rev.* **109**, 4760-4779
41. LaBauve, A. E., and Wargo, M. J. (2012) Growth and laboratory maintenance of *Pseudomonas aeruginosa*. *Curr. Protoc. in Microbiol.* **25**, 6E. 1.1-6E. 1.8

42. Glauninger, H., Zhang, Y., Higgins, K. A., Jacobs, A. D., Martin, J. E., Fu, Y., Coyne Rd, H. J., Bruce, K. E., Maroney, M. J., Clemmer, D. E., Capdevila, D. A., and Giedroc, D. P. (2018) Metal-dependent allosteric activation and inhibition on the same molecular scaffold: the copper sensor CopY from *Streptococcus pneumoniae*. *Chem. Sci.* **9**, 105-118
43. Ma, Z., Cowart, D. M., Ward, B. P., Arnold, R. J., DiMarchi, R. D., Zhang, L. M., George, G. N., Scott, R. A., and Giedroc, D. P. (2009) Unnatural amino acid substitution as a probe of the allosteric coupling pathway in a mycobacterial Cu(I) sensor. *J. Am. Chem. Soc.* **131**, 18044-18045
44. Joshi, C. P., Panda, D., Martell, D. J., Andoy, N. M., Chen, T. Y., Gaballa, A., Helmann, J. D., and Chen, P. (2012) Direct substitution and assisted dissociation pathways for turning off transcription by a MerR-family metalloregulator. *Proc. Natl. Acad. Sci. U S A* **109**, 15121-15126
45. O'Halloran, T. V., and Culotta, V. C. (2000) Metallochaperones, an intracellular shuttle service for metal ions. *J. Biol. Chem.* **275**, 25057-25060
46. Philips, S. J., Canalizo-Hernandez, M., Yildirim, I., Schatz, G. C., Mondragon, A., and O'Halloran, T. V. (2015) Allosteric transcriptional regulation via changes in the overall topology of the core promoter. *Science* **349**, 877-881
47. Wei, W., Sun, Y., Zhu, M., Liu, X., Sun, P., Wang, F., Gui, Q., Meng, W., Cao, Y., and Zhao, J. (2015) Structural Insights and the Surprisingly Low Mechanical Stability of the Au-S Bond in the Gold-Specific Protein GolB. *J. Am. Chem. Soc.* **137**, 15358-15361
48. de Vries, S. J., van Dijk, M., and Bonvin, A. M. (2010) The HADDOCK web server for data-driven biomolecular docking. *Nat. Protoc.* **5**, 883-897
49. Thaden, J. T., Lory, S., and Gardner, T. S. (2010) Quorum-sensing regulation of a copper toxicity system in *Pseudomonas aeruginosa*. *J. Bacteriol.* **192**, 2557-2568
50. Fu, Y., Tsui, H. C., Bruce, K. E., Sham, L. T., Higgins, K. A., Lisher, J. P., Kazmierczak, K. M., Maroney, M. J., Dann, C. E., 3rd, Winkler, M. E., and Giedroc, D. P. (2013) A new structural paradigm in copper resistance in *Streptococcus pneumoniae*. *Nat. Chem. Biol.* **9**, 177-183
51. Dennison, C., David, S., and Lee, J. (2018) Bacterial copper storage proteins. *J. Biol. Chem.*, jbc.TM117. 000180
52. Hmelo, L. R., Borlee, B. R., Almblad, H., Love, M. E., Randall, T. E., Tseng, B. S., Lin, C., Irie, Y., Storek, K. M., and Yang, J. J. (2015) Precision-engineering the *Pseudomonas aeruginosa* genome with two-step allelic exchange. *Nat. Protoc.* **10**, 1820
53. Choi, K. H., and Schweizer, H. P. (2006) mini-Tn7 insertion in bacteria with single *attTn7* sites: example *Pseudomonas aeruginosa*. *Nat. Protoc.* **1**, 153-161
54. Bradford, M. M. (1976) A rapid and sensitive method for the quantitation of microgram quantities of protein utilizing the principle of protein-dye binding. *Anal. Biochem.* **72**, 248-254
55. Ellman, G. L. (1959) Tissue sulfhydryl groups. *Arch. Biochem. Biophys.* **82**, 70-77
56. Wittig, I., Braun, H.-P., and Schägger, H. (2006) Blue native PAGE. *Nat. Protoc.* **1**, 418
57. Schneider, C. A., Rasband, W. S., and Eliceiri, K. W. (2012) NIH Image to ImageJ: 25 years of image analysis. *Nat. Methods* **9**, 671
58. Pfaffl, M. W. (2001) A new mathematical model for relative quantification in real-time RT-PCR. *Nucleic Acids Res.* **29**, e45-e45
59. Waterhouse, A. M., Procter, J. B., and Martin, D. M. A. (2009) Jalview Version 2—a multiple sequence alignment editor and analysis workbench. *Jalview Version 2—a multiple sequence alignment editor and analysis workbench*
60. Crooks, G. E., Hon, G., Chandonia, J.-M., and Brenner, S. E. (2004) WebLogo: a sequence logo generator. *Genome Res.* **14**, 1188-1190
61. Wei, W., Sun, Y., Zhu, M., Liu, X., Sun, P., Wang, F., Gui, Q., Meng, W., Cao, Y., and Zhao, J. (2015) Structural insights and the surprisingly low mechanical stability of the Au-S bond in the gold-specific protein GolB. *J. Am. Chem. Soc.* **137**, 15358-15361
62. Sakakibara, D., Sasaki, A., Ikeya, T., Hamatsu, J., Hanashima, T., Mishima, M., Yoshimasu, M., Hayashi, N., Mikawa, T., and Wälchli, M. (2009) Protein structure determination in living cells by in-cell NMR spectroscopy. *Nature* **458**, 102

63. Schrödinger Release 2017-3: Maestro, Schrödinger, LLC, New York, NY, 2017.
64. Jacobson, M. P., Pincus, D. L., Rapp, C. S., Day, T. J. F., Honig, B., Shaw, D. E., and Friesner, R. A. (2004) A hierarchical approach to all-atom protein loop prediction. *Proteins* **55**, 351-367
65. Van Zundert, G., Rodrigues, J., Trellet, M., Schmitz, C., Kastitis, P., Karaca, E., Melquiond, A., van Dijk, M., De Vries, S., and Bonvin, A. (2016) The HADDOCK2. 2 web server: user-friendly integrative modeling of biomolecular complexes. *J. Mol. Biol.* **428**, 720-725
66. Krissinel, E., and Henrick, K. (2007) Inference of macromolecular assemblies from crystalline state. *J. Mol. Biol.* **372**, 774-797
67. Delano, W. L. (2002) The Pymol Molecular Graphics System. <http://www.pymol.org>

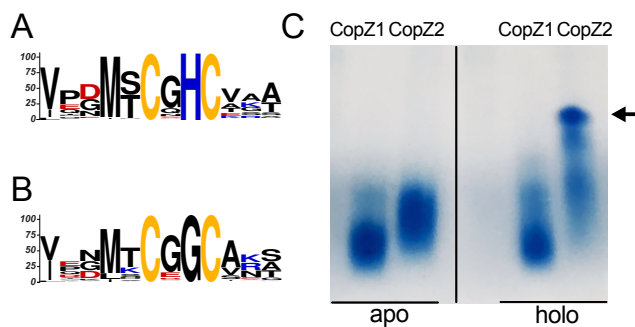


Figure 1. Structural differences of CopZ1 and CopZ2. Conserved Cu⁺ binding motifs of (A) CopZ1-like and (B) CopZ2-like proteins. (C) Native PAGE gel of purified CopZ1 and CopZ2 in the absence (left) and the presence of equimolar amount of Cu⁺ (right). The vertical dividing line in panel C indicates where the image has been spliced; all signals were from an identical original image and have not been altered. Arrow indicates multimeric structures of CopZ2.

Cytoplasmic Cu⁺ distribution in *P. aeruginosa*

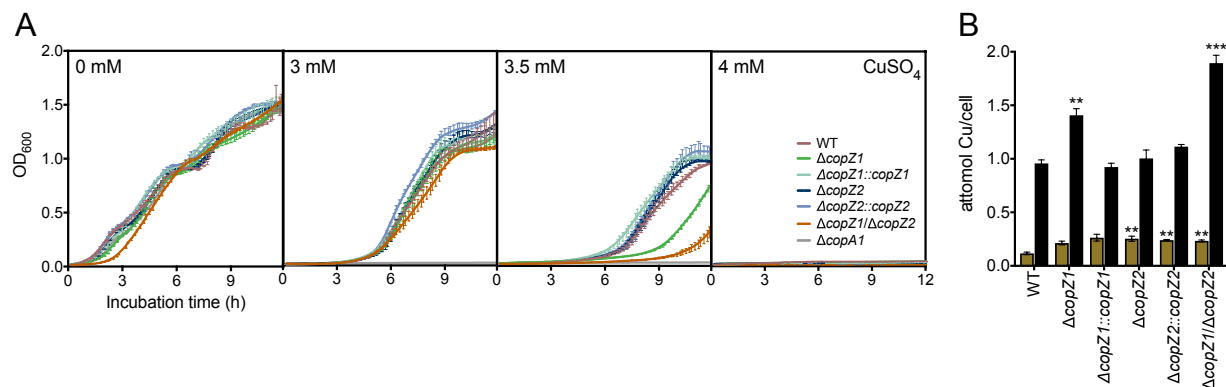


Figure 2. Contribution of CopZ1 and CopZ2 to *P. aeruginosa* Cu⁺ tolerance and metal content. (A) Growth rate of WT, $\Delta copZ1$, $\Delta copZ2$, $\Delta copZ1/\Delta copZ2$, $\Delta copA1$, as well as *copZ1* and *copZ2* complemented strains in the presence of 0 - 4 mM CuSO₄. (B) Intracellular Cu levels before (ochre) and after (black) 10 min exposure to 0.5 mM CuSO₄. Data are the mean \pm SE of three independent experiments. Significant differences from values in the WT strain as determined by unpaired two-tailed Student's t-test are ** $P < 0.01$, *** $P < 0.001$.

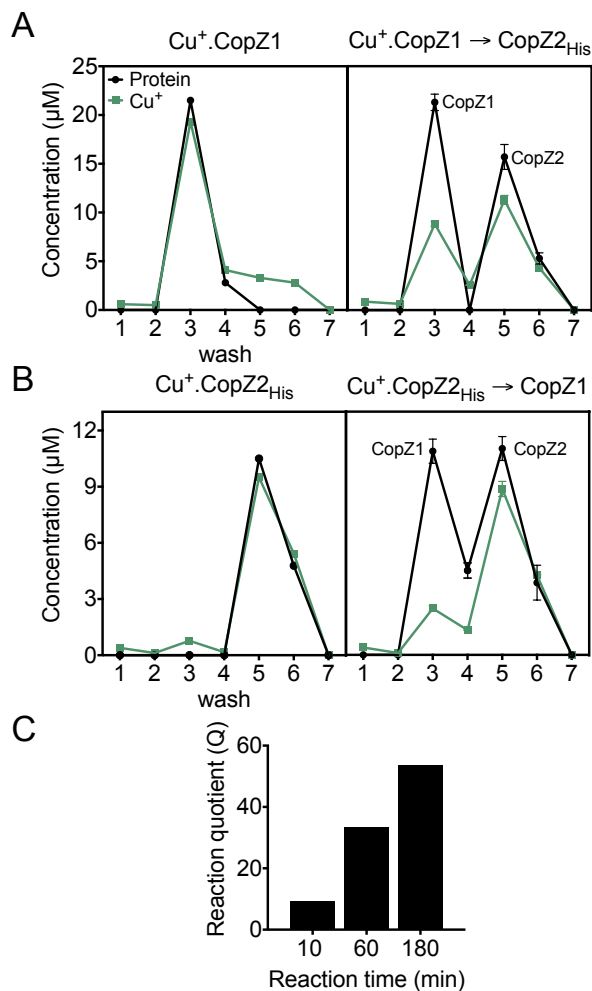


Figure 3. Cu⁺ exchange among CopZ1 and CopZ2. (A-B) Protein (black) and Cu⁺ (green) in the washes and eluates from Ni-NTA resin (wash 1-4, elution 5-7) (A) Cu⁺ transfer from CopZ1_{holo} in the absence (left) and the presence of CopZ2_{apo} (right); and (B) Cu⁺ transfer from CopZ2_{holo} in the absence (left) and the presence of CopZ1_{apo} (right). Data are the mean ± SE of three independent experiments. (C) Cu⁺ transfer reaction from CopZ1_{holo} to CopZ2_{apo} after various incubation times expressed as a reaction quotient $Q = ([\text{CopZ1}_{\text{apo}}] \cdot [\text{CopZ2}_{\text{holo}}] \cdot [\text{CopZ1}_{\text{holo}}]^{-1} \cdot [\text{CopZ2}_{\text{apo}}]^{-1})$ for $\text{CopZ1}_{\text{holo}} + \text{CopZ2}_{\text{apo}} \rightleftharpoons \text{CopZ1}_{\text{apo}} + \text{CopZ2}_{\text{holo}}$.

Cytoplasmic Cu^+ distribution in *P. aeruginosa*

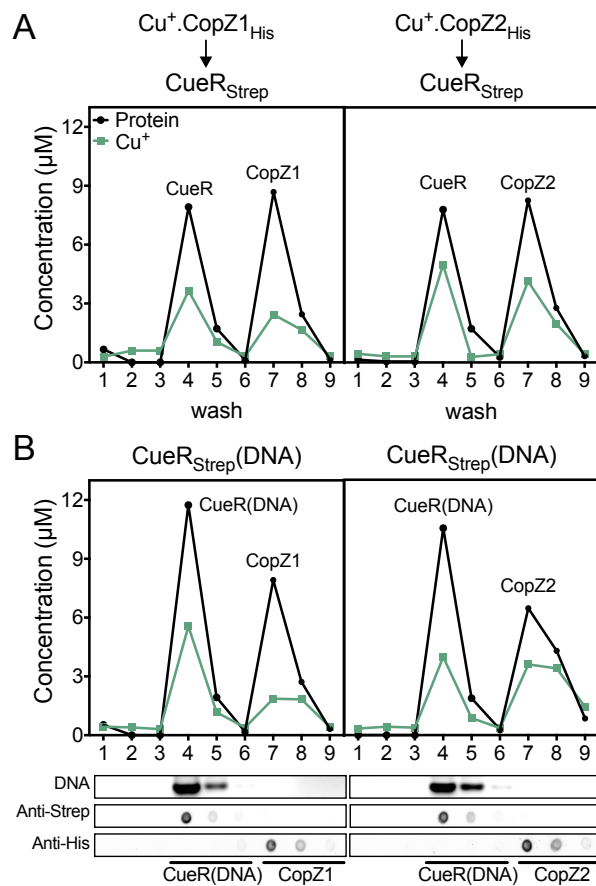


Figure 4. Cu^+ transfer from $\text{CopZs}_{\text{holo}}$ to CueR_{apo} . Experiments were performed in the absence (A) and the presence (B) of *PcopZ2*. Data are from a representative Cu^+ transfer experiment from $\text{CopZ1}_{\text{holo}}$ (left) and $\text{CopZ2}_{\text{holo}}$ (right). Protein (black) and Cu^+ (green) contents in washes and eluates from Ni-NTA resin (wash 1-6, elution 7-9). Lower panels show fractions analyzed for DNA content (top panel), Strep-tagged CueR (second panel) and His-tagged CopZs (bottom panel).

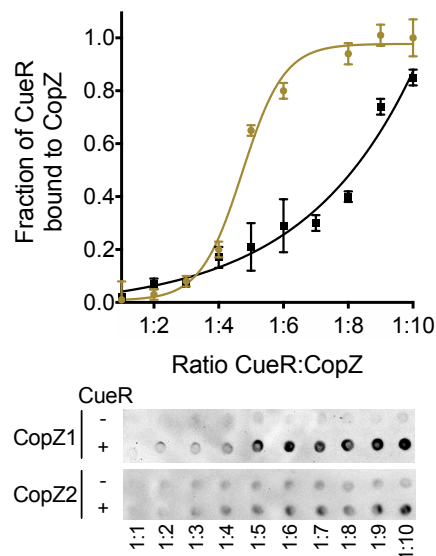


Figure 5. *In vitro* interaction between CopZs and CueR. Co-purification of isolated proteins by Strep-Tactin[®]XT batch affinity chromatography using 10 μ M Strep-tagged CueR_{apo} dimer and varying concentrations of His-tagged CopZ_{Sapo} (10-100 μ M). His-tagged proteins co-purified with CueR were immunostained to calculate their relative abundance as a measure of the fraction of CueR bound to CopZs (CopZ1 ochre and CopZ2 black). Curves were fitted to a sigmoidal equation giving a $K_{1/2}$ value of 1:4.73 \pm 0.13 for CopZ1 and \geq 1:9 for CopZ2 (units are CueR:CopZ ratios). Data are the mean of two replicates of an immunostaining representative from three independent experiments.

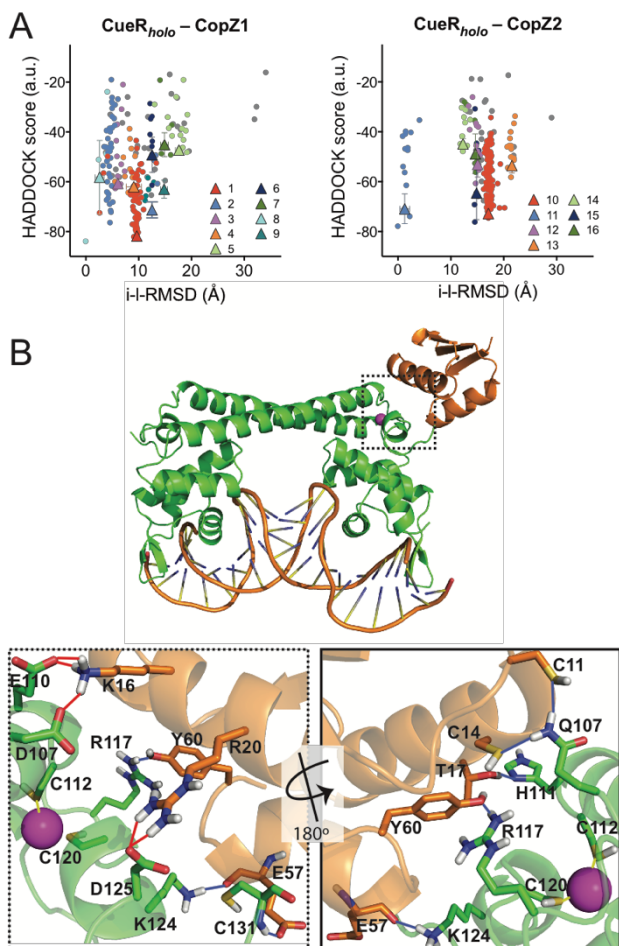


Figure 6. *In silico* CopZs interaction with CueR. (A) Intermolecular docking scores as a function of the interface-ligand RMSD for residues in the intermolecular contact area (10 Å cutoff). Individual clusters numbered as in Table S2 are indicated in various colors. Conformations that did not fit in any cluster are shown as gray dots. The clusters averages are indicated as triangles with error bars. (B) CueR_{holo}-CopZ1_{apo} interaction model. The conformer with lower HADDOCK score from cluster 1 is shown. CueR (green), CopZ1 (orange), DNA, Cu⁺ (cyan), binding residues (sticks), H-bonds (blue lines), and salt bridges (red lines) are represented. Dotted frame shows a detail of the interaction site and the continues frame a 180° rotated view (bottom panels).

Cytoplasmic Cu⁺ distribution in *P. aeruginosa*

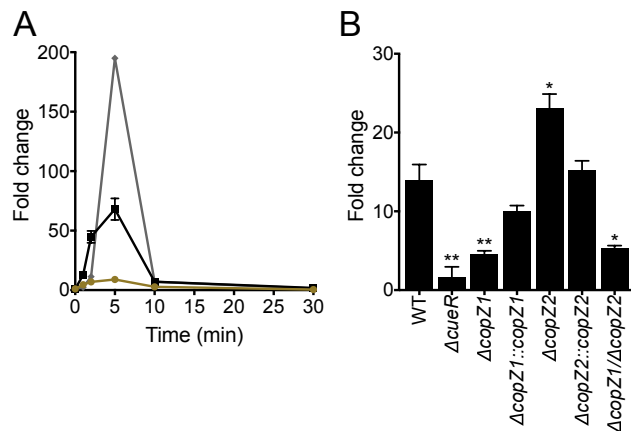


Figure 7. Transcriptional levels of *copZ1*, *copZ2*, and *copA1* upon Cu²⁺ stress. (A) Kinetics of expression at RNA level of *copZ1* (ochre circles), *copZ2* (black squares), and *copA1* (grey diamonds) upon 0.5 mM CuSO₄ treatment. (B) *copA1* expression in $\Delta cueR$, $\Delta copZ1$, $\Delta copZ2$, $\Delta copZ1/\Delta copZ2$ mutants and complemented strains after 2 min of 0.5 mM CuSO₄ treatment. Data are the mean \pm SE of three independent experiments. Significant differences from the WT as determined by unpaired two-tailed Student's t-test are * $P < 0.05$, ** $P < 0.01$.

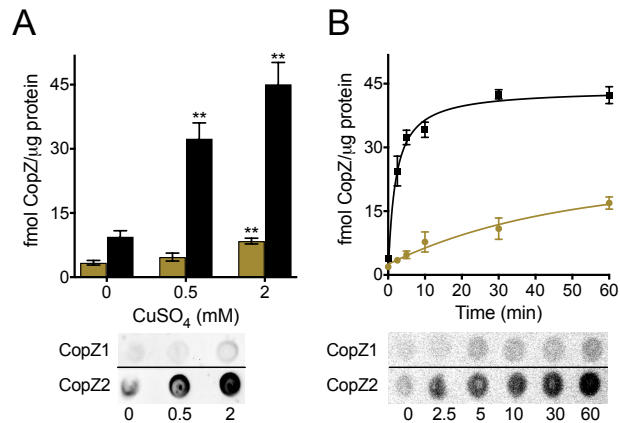


Figure 8. *In vivo* abundance of CopZ1 (ochre) and CopZ2 (black) proteins. $\Delta copZ1$ and $\Delta copZ2$ were complemented with the corresponding His-tagged gene under control of the native promoter. His-tagged proteins were immunostained and their abundance calculated using a standard curve of pure His-tagged protein. The horizontal dividing lines indicate where the images have been spliced; signals were from an identical original image and have not been altered. CopZs levels were determined after exposure to (A) different CuSO₄ concentrations during 10 min or (B) 0.5 mM CuSO₄ during different times. Data are the mean \pm SE of three independent experiments. Significant differences from values in the absence of CuSO₄ as determined by unpaired two-tailed Student's t-test are ** $P < 0.01$.

Cytoplasmic Cu⁺ distribution in *P. aeruginosa*

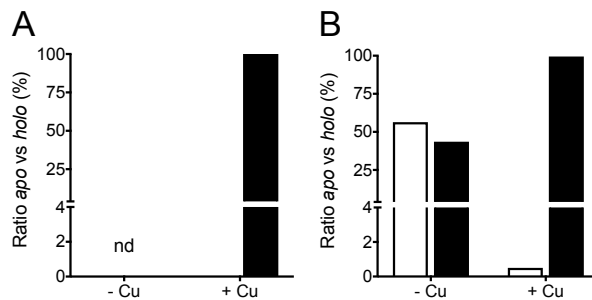


Figure 9. *Apo/olo* ratios of CopZs by alkylation-mass spectrometry analysis. $\Delta copZ$ complemented strains were cultured in absence and presence of 0.5 mM CuSO₄ during 10 min. (A) CopZ1 and (B) CopZ2, Cys were alkylated with maleimide and enriched protein preparations analyzed by MS/MS. The *apo* (white) and *olo* (black) ratios were quantified by summing the fragment intensity to obtain the molar fraction of modified vs. non-modified Cys in Cu binding site-containing peptides. Data is the average of two independent experiments.

Cytoplasmic Cu⁺ distribution in *P. aeruginosa*

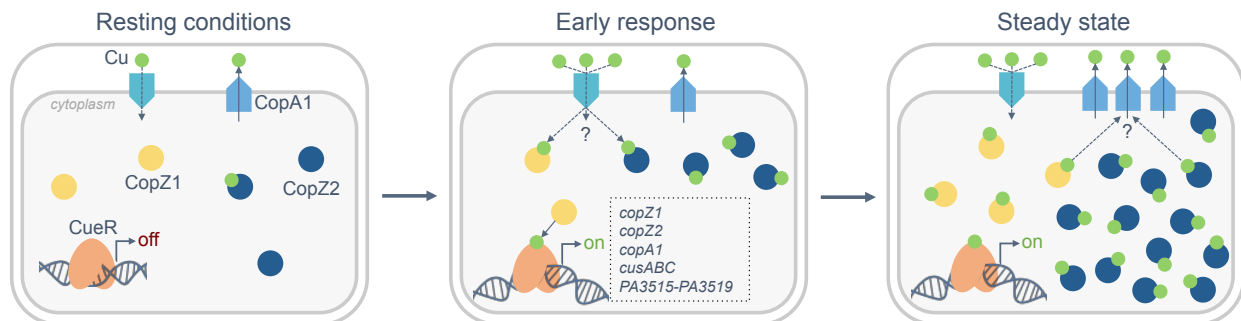


Figure 10. Model of Cu⁺ homeostasis via CopZ1, CopZ2 and CueR interplay in the cytoplasm of *P. aeruginosa*. Three different landscapes are represented. *Resting conditions* (left) in absence of Cu-stress, where CopZ1 (yellow) and CopZ2 (blue) appear to be at similar levels and CopZ2 is only partially metallated. *Early response* (central panel) takes place within 1-3 min of external Cu²⁺ exposure. Once Cu enters into the cytoplasm, CopZ1 metallates the sensor CueR (orange) leading to transcriptional activation of the CueR regulon genes (dotted box), while CopZ2 acts as an early Cu⁺ storage system. The CopZ2 pool increases immediately and become fully metallated. As *steady state* is reached (right panel), intracellular Cu⁺ and CopZ2 levels remain constant as result of equal Cu⁺ influx and efflux rates. CopZ1 and CopZ2 constitute independent Cu⁺ pools, working coordinately to maintain Cu⁺ homeostasis in the cytoplasm of *P. aeruginosa*.

The interplay of the metallosensor CueR with two distinct CopZ chaperones defines copper homeostasis in *Pseudomonas aeruginosa*

Lorena Novoa-Aponte, David Ramírez and José M. Argüello

J. Biol. Chem. published online February 4, 2019

Access the most updated version of this article at doi: [10.1074/jbc.RA118.006316](https://doi.org/10.1074/jbc.RA118.006316)

Alerts:

- [When this article is cited](#)
- [When a correction for this article is posted](#)

[Click here](#) to choose from all of JBC's e-mail alerts

Supporting Information for

The interplay of the metallosensor CueR with two distinct CopZ chaperones defines copper homeostasis in *Pseudomonas aeruginosa*

Lorena Novoa-Aponte, David Ramírez, and José M. Argüello*

From the Department of Chemistry and Biochemistry, Worcester Polytechnic Institute, 60 Prescott St, Worcester, Massachusetts, 01605, United States of America

Running title: Cytoplasmic Cu⁺ distribution in *P. aeruginosa*

*To whom correspondence should be addressed: Dr. José M. Argüello, Department of Chemistry and Biochemistry, Worcester Polytechnic Institute, 60 Prescott St, Worcester, Massachusetts, 01605, United States of America. Phone: (508) 330-5169, e-mail: arguello@wpi.edu

This PDF file includes:

Figures S1 to S6

Tables S1 to S3

References for SI citations

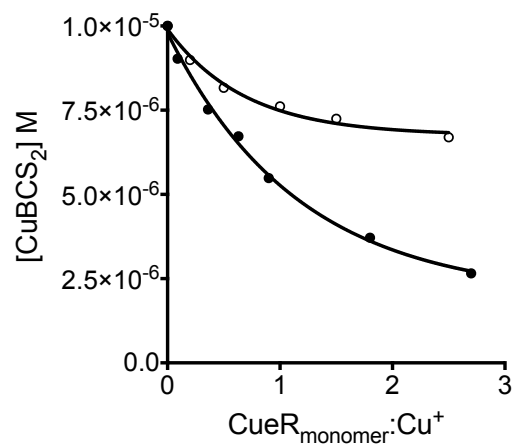


Fig. S1. CueR-Cu⁺ dissociation constant K_D determined using a BCS competition assay (2). Reaction mixtures were prepared in buffer H with constant concentrations of Cu⁺ (10 μM) and BCS (25 or 100 μM) and varying concentrations of CueR (1-30 μM monomer). After 10 min equilibration, CuBCS₂ concentrations were estimated using A_{483} (β_2 10^{19.8} M⁻², ϵ_{483} 13000 M⁻¹cm⁻¹). CueR-Cu⁺ K_D was calculated by fitting the experimental data to the equilibrium binding equation (2,3). As CueR dimers bind two Cu⁺ (4,5), $[P]_{\text{total}} = [\text{CueR monomer}]$. K_D values determined using 25 μM CuBCS₂ (black circles) and 100 μM CuBCS₂ (open circles) were curve fitted to $K_D = 3.1 \pm 0.2 \times 10^{-16}$ M and $K_D = 7.9 \pm 0.9 \times 10^{-17}$ M, respectively. An average $K_D = 2.5 \pm 1.0 \times 10^{-16}$ M was calculated based on 6 independent experiments.

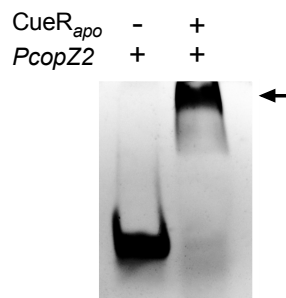


Fig. S2. Interaction CueR_{apo}-*PcopZ2* examined by Electrophoretic Mobility Shift Assay. 10 pmol of 50-bp unlabeled *PcopZ2* (Table S1) were incubated 30 min at room temperature with 500 pmol CueR dimer in 10 mM Tris (pH 7.5), 100 mM NaCl, 1 mM EDTA, 0.1 mM DTT, 5% glycerol, 0.01 mg/mL BSA. The electrophoretic mobility of *PcopZ2* in the absence (left) and the presence of CueR_{apo} (right), was observed in 10% polyacrylamide/TAE gels stained with ethidium bromide. The arrow highlights the mobility shift of *PcopZ2* in the presence of CueR.

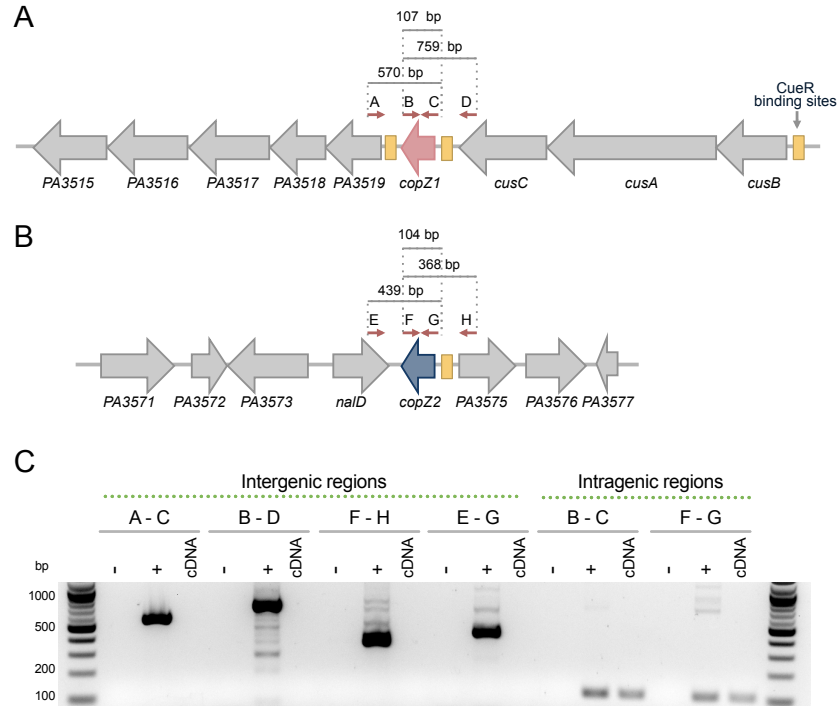


Fig. S3. *P. aeruginosa* *copZ1* and *copZ2* operon mapping. Total RNA from *P. aeruginosa* PAO1 in exponential growth phase was reverse transcribed and the cDNA used as template for PCR. Primers were designed in order to amplify the junctions between adjacent genes. Primers in intragenic regions were included as controls (Table S1). Schematic representation of the position of primers designed for co-transcription analysis of the gene cluster of (A) *copZ1* and (B) *copZ2* operons. (C) Each panel is constituted by three lanes: negative control, H₂O; gDNA lane, which contains amplified products from genomic DNA and serves as positive control; and the cDNA lane, that contains the RT-PCR products.

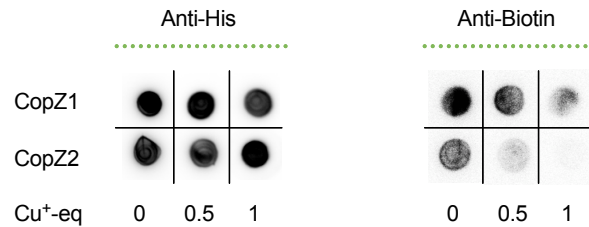


Fig. S4. Cu⁺ protection of Cys residues at the metal binding sites from biotin-maleimide alkylation. Pure extracts of His-tagged CopZ1 and CopZ2 were separately alkylated with biotin-maleimide in the presence of 0, 0.5, and 1 eq of Cu⁺. After removing excess of alkylating agent by Ni-NTA affinity chromatography, proteins were dot-blotted and immune stained either with anti-His antibodies or anti-Biotin antibodies. The dividing lines indicate where the images have been spliced; signals were from an identical original image and have not been altered. A decrease in anti-biotin staining indicated that Cu⁺ protects Cys against chemical modification.

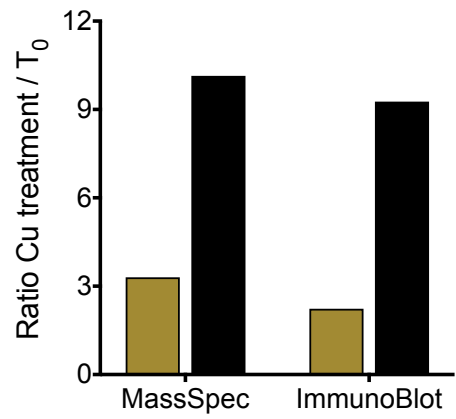


Fig. S5. Levels of CopZ1 (ochre) and CopZ2 (black) in the presence of 0.5 mM CuSO₄ (10 min) relative to those in the absence of metal, determined by MS/MS and immunostaining. Relative ratios in MS/MS were generated by spectral counts (total spectra). In both approaches, samples were normalized prior to the experiment (equal cell counts).

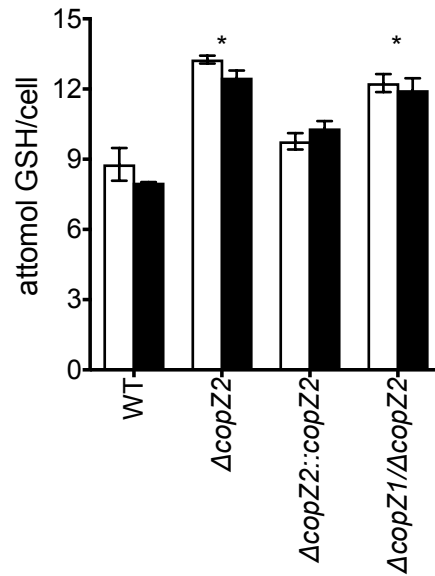


Fig. S6. Levels of GSH in WT, $\Delta copZ2$, $\Delta copZ1/\Delta copZ2$ mutant strains and *copZ2* complemented strain upon 0.5 mM $CuSO_4$ treatment (10 min). The amounts of total GSH in the absence (white) and the presence of copper (black) were measured spectrophotometrically using a kinetic assay of DNTB reduction coupled to GSSG recycling. Cells were incubated in 0.5 mM $CuSO_4$ in antibiotic-free LB medium. 2 mL aliquots were taken before and after 10 min of $CuSO_4$ addition, harvested by centrifugation, resuspended in 150 μ L 5% sulfosalicylic acid, sonicated 30 sec in a dry-ice/ethanol bath, and incubated for 10 min on ice. Cellular debris and proteins were removed by centrifugation at 10,000 rpm for 10 min, and supernatants used for total GSH quantification. 20 μ L samples were pre-incubated 5 min with 78 μ M DTNB, 0.115 units/mL GSH reductase, 100 mM Na_2HPO_4/Na_2HPO_4 (pH 7), 1 mM EDTA. Upon addition of 46 μ M NADPH, A412 was measured at 1 min intervals for 7 minutes. 0-200 μ M GSH in 5% sulfosalicylic acid were used as standards. Data are the mean \pm SE of three independent experiments. Significant differences from the WT as determined by paired two-tailed Student's t-test are * $P < 0.05$.

Table S1. Bacterial strains, plasmids and primers used in this study

Strains	Relevant features	Reference
<i>Pseudomonas aeruginosa</i>		
PAO1	Wild type	(6)
$\Delta copZ1$	<i>copZ1</i> gene replaced by a <i>Bam</i> HI site	(7)
$\Delta copZ1::copZ1$	<i>copZ1</i> complemented gene, C-terminal TEV_His-tag, under endogenous promoter, Gm ^R	This study
$\Delta copZ2$	<i>copZ2</i> gene interrupted by a <i>Pvu</i> II site and a stop codon	This study
$\Delta copZ2::copZ2$	<i>copZ2</i> complemented gene, C-terminal TEV_His-tag, under endogenous promoter, Gm ^R	This study
$\Delta copZ1/\Delta copZ2$	<i>copZ2</i> gene interrupted by a <i>Pvu</i> II site and a stop codon in the $\Delta copZ1$ background	This study
$\Delta copA1$	PW7626, <i>copA1</i> (PA3920)::ISphoA::Tet ^R	(8)
$\Delta cueR$	PW9026, <i>cueR</i> (PA4778)-B07::ISphoA/hah::Tet ^R	(8)
<i>Escherichia coli</i>		
BL21(DE3)	<i>F⁻ ompT gal dcm lon hsdS_B(r_B⁻m_B⁻) λ(DE3 [<i>lacI lacUV5-T7p07 ind1 sam7 nin5</i>] [<i>malB⁺</i>]_{K-12}(λ^S))</i>	Novagen
BL21(DE3)pLysS	BL21(DE3) strain <i>pLysS</i> [<i>T7p20 ori_{p15A}</i>](<i>Cm^R</i>)	Novagen
Top10	<i>F⁻ mcrA Φ80lacZΔM15 ΔlacX74 recA1 araD139 Δ(ara-leu)7697 galU galK rpsL (Str^R) endA1 nupG</i>	Invitrogen
S17.1	<i>Tp^R Sm^R recA, thi, pro, hsdR⁺ M⁺ RP4- 2</i> <i>Tc:Mu::Kan::Tn7/λpir.</i>	(9)
Plasmids	Relevant features	Reference
pET-30b+	T7 promoter, <i>lac</i> operator, 6xHis tag, <i>lacI</i> , Kan ^R	Novagen
<i>copZ1::pET-30b+</i>	<i>PA3520::pET-30b+</i> , Kan ^R	(2)
<i>copZ2::pET-30b+</i>	<i>PA3574.1::pET-30b+</i> , Kan ^R	(2)
pBADtopo	<i>araBAD</i> promoter, V5 epitope tag, 6xHis tag, Amp ^R	Invitrogen
<i>cueR</i> strep::pBAD	<i>PA4778_strep::pBAD</i> , Amp ^R	This study
pDONRPEX18Gm	Gateway allelic exchange vector, Gm ^R	(10)
pUC18-mini-Tn7-Gm	Suicide delivery vector, Gm ^R	(11)
pTNS2	Helper plasmid (TnsABCD site), Amp ^R	(12)
Primers	Sequence (5'-3')	
<i>copZ2</i> mutant		
CopZ2upF-GWB1	ggggacaagttgtacaaaaagcaggctacatcagcaccgctacagcag	
CopZ2upR01	cagctgtcagggctggccggcgctcatccctgaaccttgaaa	
CopZ2downF01	gcccggccagcctgacagctggtacggcgatcacccatgc	
CopZ2downR-GWB2	ggggaccactttgtacaagaagctgggtagcggctgctactggcacttc	
Mutant complementation		
Comp_CopZ1_F	ttttactagtctggcgggatacctcgtc	
Comp_CopZ1_R	ttttggtacctcaatgatgatgatgatgggactgaaaatacaggtttcggcgtgctacggccctccggataaccgg	
Comp_CopZ2_F	ttttactagtctggcgggatacctcgtc	
Comp_CopZ2_R	ttttggtacctcaatgatgatgatgatgggactgaaaatacaggtttcggcgtgctgcccagctcggcggcgtg	
<i>copZ2</i> promoter		
<i>copZ2</i> prom_F	tatttcgaggattgacctgacaccatgtcaaggtcgaatacggccat	
<i>copZ2</i> prom_R	atggggcgattttcggcctgacattggtgtcaaggtcaatcctcgaata	
Operon mapping		
OW_PA3519_to_copZ1 (A)	tgtaacggattgaagtcat	
OW_PA3521_to_copZ1 (D)	agcgcgacagtcgctcctga	
OW_PA3575_to_copZ2 (H)	gaatagcggcgatggacat	
OW_PA3574_to_copZ2 (E)	gcccgcatectgacctcc	
qPCR		
qPA4268F	gcaaaactgcccgaacgtc	
qPA4268R	tacacgaccgcccaggtatca	
qCopZ1F (C)	aagactgtcaccgtatcct	
qCopZ1R (B)	aatgcgtgcttgcaga	
qCopZ2F (G)	ggtgcaggcgaaggatt	
qCopZ2R (F)	ggatcgctcgagtacct	
qCopA1F	gaaacgggtgctggcgaagat	
qCopA1R	ttaaccaggcctgctccag	

Table S2. Docking studies of CopZ1 and CopZ2 with CueR.

CueR_{holo} – CopZ1							
Cluster		HADDOCK	RMSD	vdW	Electrostatic	Desolvation	Z
No.	Size	a.u.	Å	kcal/mol	kcal/mol	kcal/mol	
1	56	-82 ± 1	3.9 ± 0.2	-29 ± 2	-324 ± 8	12 ± 2	-2.0
2	41	-71 ± 3	2.0 ± 0.1	-37 ± 4	-195 ± 59	4 ± 10	-1.0
3	20	-61 ± 2	2.6 ± 0.2	-28 ± 3	-179 ± 34	3 ± 8	-0.1
4	16	-62 ± 2	3.6 ± 1.1	-27 ± 5	-231 ± 30	11 ± 3	-0.2
5	15	-47 ± 1	7.1 ± 0.5	-28 ± 5	-132 ± 18	7 ± 6	1.1
6	8	-49 ± 7	5.3 ± 0.1	-38 ± 5	-96 ± 19	7 ± 3	1.0
7	5	-45 ± 5	6.2 ± 0.5	-28 ± 4	-106 ± 23	4 ± 4	1.3
8	5	-58 ± 15	1.1 ± 0.7	-34 ± 4	-179 ± 43	12 ± 8	0.1
9	4	-63 ± 4	4.8 ± 0.2	-27 ± 5	-268 ± 34	11 ± 7	-0.3
Average cluster size ± SD = 18.9 ± 18.1							
CueR_{holo} – CopZ2							
Cluster		HADDOCK	RMSD	vdW	Electrostatic	Desolvation	Z
No.	Size	a.u.	Å	kcal/mol	kcal/mol	kcal/mol	
10	113	-73 ± 1	7.4 ± 0.1	-32 ± 7	-183 ± 22	-5 ± 4	-1.4
11	14	-71 ± 6	0.1 ± 0.3	-34 ± 4	-242 ± 70	9 ± 8	-1.2
12	13	-53 ± 5	5.7 ± 0.1	-29 ± 4	-81 ± 24	-8 ± 5	0.5
13	13	-54 ± 3	8.6 ± 0.1	-30 ± 4	-152 ± 25	6 ± 7	0.5
14	9	-45 ± 2	4.3 ± 0.1	-35 ± 3	-44 ± 10	-1 ± 5	1.3
15	6	-65 ± 11	6.5 ± 0.1	-35 ± 2	-215 ± 30	10 ± 6	-0.6
16	6	-49 ± 8	6.0 ± 0.1	-26 ± 3	-186 ± 28	12 ± 4	0.9
Average cluster size ± SD = 24.9 ± 39.0							

HADDOCK: HADDOCK score in a.u. (arbitrary units); **RMSD**: Root-mean-square deviation from the overall lowest-energy structure; **vdW**: van der Waals; **Z**: Z-Score indicates how many SD from the average the cluster is located in terms of score (negative values indicate stronger simulation). Significant conformational clusters are highlighted in grey.

Table S3. Interacting residues of CopZ1 and CopZ2 with CueR

CueR_{holo} – CopZ1					
Hydrogen bond			Salt bridges		
CueR	Distance (Å)	CopZ1	CueR	Distance (Å)	CopZ1
Asp107	1.7	Lys16	Asp107	2.6	Lys16
Glu110	1.7	Lys16	Glu110	4.0	Lys16
His111	2.0	Thr17	Glu110	2.7	Lys16
Gln113	2.2	Cys11	Asp125	2.8	Arg20
Gln113	2.2	Cys14	Asp125	3.6	Arg20
Arg117	2.0	Tyr60	Asp125	3.0	Arg20
Lys124	1.7	Glu57	Asp125	3.4	Arg20
Asp125	1.9	Arg20			
Asp125	2.2	Arg20			
Cys131	3.0	Glu57			

CueR_{holo} – CopZ2					
Hydrogen bond			Salt bridges		
CueR	Distance (Å)	CopZ2	CueR	Distance (Å)	CopZ2
Glu110	2.2	Cys11	Lys124	3.8	Glu58
Arg117	2.1	Gly8	Lys124	2.6	Glu58
Arg117	2.4	Thr10			
Arg117	1.8	Thr10			
Asp119	1.7	Tyr60			
Lys124	1.6	Glu58			
Cys131	1.7	Glu58			

References

1. Letunic, I., and Bork, P. (2006) Interactive Tree Of Life (iTOL): an online tool for phylogenetic tree display and annotation. *Bioinformatics* **23**, 127-128
2. Quintana, J., Novoa-Aponte, L., and Argüello, J. M. (2017) Copper homeostasis networks in the bacterium *Pseudomonas aeruginosa*. *J. Biol. Chem.* **292**, 15691-15704
3. Xiao, Z., Brose, J., Schimo, S., Ackland, S. M., La Fontaine, S., and Wedd, A. G. (2011) Unification of the copper(I) binding affinities of the metallo-chaperones Atx1, Atox1, and related proteins: detection probes and affinity standards. *J. Biol. Chem.* **286**, 11047-11055
4. Changela, A., Chen, K., Xue, Y., Holschen, J., Outten, C. E., O'Halloran, T. V., and Mondragon, A. (2003) Molecular basis of metal-ion selectivity and zeptomolar sensitivity by CueR. *Science* **301**, 1383-1387
5. Philips, S. J., Canalizo-Hernandez, M., Yildirim, I., Schatz, G. C., Mondragon, A., and O'Halloran, T. V. (2015) Allosteric transcriptional regulation via changes in the overall topology of the core promoter. *Science* **349**, 877-881
6. Winsor, G. L., Griffiths, E. J., Lo, R., Dhillon, B. K., Shay, J. A., and Brinkman, F. S. (2015) Enhanced annotations and features for comparing thousands of *Pseudomonas* genomes in the *Pseudomonas* genome database. *Nucleic Acids Res.* **44**, D646-D653
7. Thaden, J. T., Lory, S., and Gardner, T. S. (2010) Quorum-sensing regulation of a copper toxicity system in *Pseudomonas aeruginosa*. *J. Bacteriol.* **192**, 2557-2568
8. Jacobs, M. A., Alwood, A., Thaipisuttikul, I., Spencer, D., Haugen, E., Ernst, S., Will, O., Kaul, R., Raymond, C., Levy, R., Chun-Rong, L., Guenther, D., Bovee, D., Olson, M. V., and Manoil, C. (2003) Comprehensive transposon mutant library of *Pseudomonas aeruginosa*. *Proc. Nat. Acad. Sci. USA* **100**, 14339-14344
9. Simon, R., Priefer, U., and Puhler, A. (1983) A broad host range mobilization system for *In vivo* genetic-engineering-transposon mutagenesis in gram-negative bacteria. *Nat. Biotechnol.* **1**, 784-791
10. Hmelo, L. R., Borlee, B. R., Almblad, H., Love, M. E., Randall, T. E., Tseng, B. S., Lin, C., Irie, Y., Storek, K. M., and Yang, J. J. (2015) Precision-engineering the *Pseudomonas aeruginosa* genome with two-step allelic exchange. *Nat. Protoc.* **10**, 1820
11. Choi, K. H., and Schweizer, H. P. (2006) mini-Tn7 insertion in bacteria with single *attTn7* sites: example *Pseudomonas aeruginosa*. *Nat. Protoc.* **1**, 153-161
12. Choi, K.-H., Gaynor, J. B., White, K. G., Lopez, C., Bosio, C. M., Karkhoff-Schweizer, R. R., and Schweizer, H. P. (2005) A Tn7-based broad-range bacterial cloning and expression system. *Nat. methods* **2**, 443